ENHANCEMENT OF VASCULAR STABILITY THROUGH ARF6 DEACTIVATION REDUCES INFLAMMATORY PATHOLOGIES

by

Chadwick Thelen Davis

A dissertation submitted to the faculty of
The University of Utah
in partial fulfillment of the requirements for the degree of

Doctor of Philosophy

Department of Human Genetics

The University of Utah

August 2014

The University of Utah Graduate School

STATEMENT OF DISSERTATION APPROVAL

The dissertation of **Chadwick Thelen Davis**

has been approved by the following supervisory committee members:

Dean Y. Li	, Chair	**5/22/2014** Date Approved
L. Charles Murtaugh	, Member	**5/22/2014** Date Approved
Gabrielle Kardon	, Member	**5/22/2014** Date Approved
Gillian Stanfield	, Member	**5/22/2014** Date Approved
Vicente Planelles	, Member	**5/22/2014** Date Approved

and by **Lynn Jorde** , Chair/Dean of

the Department/College/School of **Human Genetics**

and by David B. Kieda, Dean of The Graduate School.

ABSTRACT

The vasculature infuses nearly every tissue with oxygen and nutrients. It facilitates the transport of cells and chemical messages throughout the body and maintains proper fluid balance in the individual tissues. During angiogenesis and inflammation, vessels that compose the vasculature display enhanced permeability. This leak is regulated by the monolayer of endothelial cells that line each vessel. This thesis aims to further describe the molecular mechanisms within endothelial cells that control vascular leak. I present our research identifying a molecular signaling axis that controls vascular leak induced by inflammatory cues through the small GTPase ADP-ribosylation factor 6 (ARF6). We show that blockade of ARF6 enhances endothelial barrier function, reduces vascular leak, and prevents inflammatory pathology.

We identify a signaling axis composed of Myeloid Differentiation Factor 88 (MYD88), ARF-Nucleotide Binding Site Opener (ARNO), and ARF6 in endothelial cells that is used by the inflammatory cytokine, interlukin-1β (IL-1β), to dissociate cell junctions and enhance vascular leak. We determined that IL-1β enhances permeability rapidly, independently of gene-expression changes, and in a manner dependent on ARF6 activation. We showed that ARF6 activation induced the dissociation of the cell junction protein vascular endothelial cadherin (VE-Cadherin) and when ARF6 was blocked, VE-Cadherin dissociation was prevented and vascular permeability was

reduced. Inhibiting this signaling axis in mice with a small molecule inhibitor reduced vascular leak and inflammatory pathologies associated with arthritis.

MYD88 is a crucial adapter protein for many inflammatory pathways, including the Toll-like-receptors (TLRs). TLRs are the primary receptors that detect pathogens by recognizing danger-associated molecular patterns (DAMPs) such as bacterial lipopolysaccharaides (LPS) and initiating an inflammatory cascade. We determined that the MYD88-ARNO-ARF6 cascade is also responsible for vascular leak induced by LPS. We characterized the peptide MyrARF6 2-13 as an inhibitor of ARF6 activation and showed that peptide treatment is sufficient to reduce vascular leak and enhance survival of mice in experimental sepsis.

We suggest that ARF6 controls inflammatory pathology independent of inflammatory factors such as cytokines. Such observations suggest that vascular leak itself could be a key driver of inflammatory pathology and may pave the way for the development of therapeutics that do not leave patients immunocompromised.

.

This dissertation is dedicated to my wife, my children, and my parents. You gave so much so that I could succeed. One day I hope to return the favor.

"A discovery in science, or a new theory, even when it appears most unitary and most all-embracing, deals with some immediate element of novelty or paradox within the framework of far vaster, unanalyzed, unarticulated reserves of knowledge, experience, faith, and presupposition. Our progress is narrow; it takes a vast world unchallenged and for granted. This is one reason why, however great the novelty or scope of new discovery, we neither can, nor need, rebuild the house of the mind very rapidly. This is one reason why science, for all its revolutions, is conservative. This is why we will have to accept the fact that no one of us really will ever know very much. This is why we shall have to find comfort in the fact that, taken together, we know more and more."

Julius Robert Oppenheimer 1904-1967

"Science never solves a problem without creating ten more."

George Bernard Shaw 1856-1950

TABLE OF CONTENTS

ACKNOWLEDGEMENTS

I wish to thank the many people that contributed to this work and helped me succeed. First, the members of the Li Lab who adopted me into their family and made me realize I was capable of more than I thought possible and would not accept anything less: Dean Li, Chris Gibson, Shannon Odelberg, Allie Grossman, Matt Smith, Aubrey Chan, Weiquan Zhu, Jing Ling, Nyall London, Allie Grossman, Kirk Thomas, Sutip Navankasattusas, Jay Bowman-Kirigin, Tara Mleynek, Jae Hyuk-Yoo, Lise Sorensen, Amy Lim, Nikolaos Diakos, Stavros Drakos, Dallas Shi, Huiming Sun, Zhengfu Tai, Shawn Guo, Aaron Rogers, and Meghan Woolley. I also would like to thank the many other people that helped out in various capacities: my committee members past and present, Charles Murtaugh, Gabrielle Kardon, Gillian Stanfield, Vicente Planelles, and Anne Moon; and the other sages whose wisdom and guidance I received throughout the years: Guy Zimmerman, Robert Campbell, Dri Abreu, Claudia Araujo, Scott Endicott, Kevin Whitehead, Paul Randazzo, Richard Kahn, Chad Huff, Tatum Simonson, and Lynn Jorde. Finally, the administrators who helped keep my act together: Linn Steele, Julia Pili, Susan Kazaryan, Elaine Fry, and Natalie Johnson.

CHAPTER 1

INTRODUCTION

In mammals, the vasculature is an essential network composed of blood vessels that infuse nearly every tissue. This ubiquitous placement throughout the body makes it at least tangentially involved in almost all described pathology. The vasculature is responsible for the transport of oxygen, nutrients, and leukocytes at proper levels into the appropriate tissues at the appropriate times. Lining the vasculature are endothelial cells that maintain barrier function to control the passage of the transported constituents while maintaining proper fluid balance in the tissues. In order to regulate barrier function, endothelial cells modulate transcytosis, fenestrae, and cell-cell junction molecules such as adherens and tight junctions. Vascular barrier function is directly responsible for controlling swelling, one of the five cardinal signs of inflammation. The endothelial signaling mechanisms by which this permeability occurs and the contribution of vascular permeability to disease pathology are poorly described.

Vascular leak has been observed in nearly all described inflammatory pathologies; key examples include infection, trauma, cancer, epilepsy, and autoimmune diseases such as arthritis and multiple sclerosis (MS)[1]. Vascular leak is often localized to the site of infection and immune response. For example, in conditions such as arthritis or MS, the vascular leak is limited to either the problematic joints or isolated areas of the central

nervous system. The same is true for epilepsy and localized infections where vascular leak is limited to the epileptic foci or the site of infection. In instances such as severe flu, the vascular leak in the lungs can be so extreme that oxygen exchange with the blood is inhibited and the patient suffocates [2]. Infections and immune responses can also become disseminated and induce systemic inflammatory responses, causing widespread vascular leak[3]. Conditions such as viral hemorrhagic fever and bacteremia induce such profound disseminated vascular leak that shock is induced from the reduced blood volume and tissues cannot properly transport nutrients and oxygen. Currently, the primary treatments for such disseminated inflammatory conditions include fluid replacement therapy, administration of the appropriate antibiotics, and in some cases, anti-inflammatories [1a, 4]. However, with these treatment options, morbidity and mortality are still very high and novel approaches need to be developed. One potential strategy may be to directly block inflammatory vascular leak and prevent excess fluid from disrupting tissue and organ function while allowing the canonical inflammatory response to progress uninhibited.

The mechanisms of vascular leak

In order for fluid to leave the vasculature and enter the periphery, it has to cross a monolayer of endothelial cells. Fluid can cross the endothelial monolayer in a transcellular manner (directly through cells) or in a paracellular manner (around individual cells). Trancellularly passage occurs either through endothelial fenestrae, in which a single endothelial cell resembles a sieve, or through caveolae-mediated vesicular transport [5] (Figure 1.1).

Endothelial fenestrae are present only on specialized tissues where molecular exchange with the blood is common, such as within the endocrine system and the kidneys. Although many signaling mechanisms can facilitate caveolae-mediated vesicular transport, one of the best-documented examples is albumin-stimulated transcytosis. Free albumin binds to and stimulates the transmembrane receptor gp60 on the luminal side of the endothelial membrane, which releases activated $G\alpha_i$ and c-Src into the cytosol. c-Src is then free to phosphorylate Cav-1 and dynamin, leading to the assembly of dynamin at the caveolar neck and initiation of caveolar scission. This also nonspecifically captures unbound, fluid-phase proteins in the vesicle. The vesicle and its contents are then transported to the abluminal side of the cell where it fuses with the membrane and contents are released [5]. Fluid-phase proteins are more accessible to the endocytic vesicle if they display a Stokes-Einstein radius of 3.6nm (about 60 kDa) or lower Figure 1.2 [6].

Fluid and molecules also exit the vasculature between endothelial cells in a paracellular manner. Complex networks of intercellular junctional protein linkages join the endothelial cells within the monolayer and help prevent leak. The two types of junction proteins on endothelial cells that control permeability are adherens junctions and tight junctions. Adherens junctions such as vascular-endothelial cadherin (VE-Cadherin) are stabilized by linkages to cytoskeletal backbone, initiate cell-cell contacts, and promote junctional maturation [7]. Endothelial tight junction proteins such as the Zona Occludens (ZO) family and the Claudins enhance junctional stabilization on more mature junctions and do not assemble without the presence of VE-Cadherin [7]. Endothelial cell contractility mediated by force generation of myosin light chain (MLC) on the actin fibers has also been implicated in endothelial permeability [8]. However, the relationship of

cell contractility by MLC to actin and junction protein stabilization by actin remains poorly understood.

The regulation of vascular leak

Regulation of endothelial permeability through cell-cell junctions is highly complex and dynamic, involving both transcription-dependent and -independent mechanisms. For example, binding of the transcription factors Forkhead Box factor (FOX01) and beta-catenin to the claudin-5 promoter blocks transcription of claudin-5 mRNA and reduces claudin-5 levels at the cell junction [9]. Tyrosine phosphorylation of VE-Cadherin is the best-characterized mechanism of regulating VE-Cadherin presence at the cell junction. Kinases such as the Src, c-Src, and proline-rich tyrosine kinase 2 (PYK2) and phosphatases like vascular endothelial protein tyrosine phosphatase (VE-PTP) mediate the phosphorylation of VE-Cadherin depending on the permeability-enhancing stimulant [10]. In addition to the direct phosphorylation of VE-Cadherin, phosphorylation of the catenins that facilitate VE-Cadherin attachment to the cytoskeleton has also been documented to release VE-Cadherin from the cell junction. For example, proline-rich tyrosine kinase 2 (PYK2) phosphorylates beta-catenin and releases it from VE-Cadherin [11].

Regulating the kinases and phosphates that control VE-Cadherin phosphorylation and leak are a vast array of endothelial receptors that respond to autocrine, exocrine, and paracrine signals such as growth factors, inflammatory cytokines, and many other classes of ligands. For example, the permeability-enhancing stimulants VEGF through VEGFR, a receptor tyrosine kinase, and thrombin through its G-protein coupled receptor both

disrupt VE-Cadherin function [12]. Conversely, there are cues that enhance VE-Cadherin deposition at endothelial cell junctions. These include angiopoietin through its receptor Tie2, which prevents SRC-mediated VE-Cadherin phosphorylation [13], and Slit2 through the Robo4 receptor [14]. Robo4-dependent endothelial stabilization is dependent on its ability to recruit a GTPase activating protein (GAP), G-protein-coupled receptor kinase interacting 1 (GIT1) to deactivate the small GTPase ADP-ribosylation factor 6 (ARF6) [15].

The ARF-family of proteins are members of the RAS-superfamily of GTPases and are major components of the vesicular trafficking system. ARF6 activation is controlled by guanine nucleotide exchange factors (GEFs) and GTPase activating proteins (GAPs). GEFs such as Arf-Nucleotide binding site Opener (ARNO) facilitate replacement of guanosine di-phosphate with guanosine tri-phosphate onto the GTPase. This exchange induces a conformational change that is traditionally classified as an active conformation [16]. GAPs such as GIT1 induce the intrinsic GTPase activating activity of ARF6 that initiates the removal of a phosphate from GTP inducing a deactivated state conformational change [17]. ARF6 is typically present on the plasma membrane and endocytic vesicles and is an important activator of phosphatidylinositol 4-phosphate 5-kinase-α PI(4)P5α and PI(4,5)P_2 synthesis [18]. ARF6 is also necessary for internalization and downstream signaling cascades induced by many receptors, including epidermal growth factor receptor (EGFR)[19], vascular endothelial growth factor receptor 2 (VEGFR2)[20], and insulin receptor complex signaling [21]. A role for ARF6 in the regulation of vascular leak and the internalization of endothelial adherens junction proteins was only recently implicated by its necessity for proper Robo4-dependent Slit2 signaling [14].

Vascular leak is a common observation in numerous inflammatory pathologies, but the contribution of vascular leak to disease remains poorly described. Pro-inflammatory stimuli such as interleukin-1β, interleukin-6, TNF-α, and bacterial lipopolysaccharides are all sufficient to induce endothelial permeability in both cell culture and live animal models. Additionally the blockade of the cytokine receptors results in a reduction in pathology in many inflammatory models [1e, 5, 22]. For example blockade of IL-1β, TNF-α, and IL-6 signaling cascades in arthritis reduces pathology in animal models as well as human patients [1e, 23]. Similar results are often observed in sepsis, a condition in which the vascular leak is so immense that death is precipitated from shock induced by the lack of blood volume [1a, 4a, 22b, 24]. However, conflicting data and phase-III clinical trials suggest that such broad anti-inflammatory interventions still allow for substantial mortality and, especially when given chronically, leave individuals immunocompromised and susceptible to dangerous side effects such as inability to clear infection [4a, 25]. It is possible that by further defining the signaling pathways responsible for the induction of vascular leak by these pro-inflammatory cues, we may uncover a branchpoint by which vascular leak uncouples from the other inflammatory processes. We may then be able to pharmacologically target these signaling pathways to reduce vascular leak and determine, at least in part, the contribution of vascular leak to disease pathology.

Summary

This thesis describes the identification of a novel branch to the signaling cascades induced by IL-1β and bacterial lipopolysaccharides (LPS) that control vascular leak. We

have identified an association by which MYD88, a critical scaffold protein for IL-1R and TLR signal transduction, which links ARNO to the receptors, leading to ARF6 activation and paracellular vascular leak through the internalization of VE-Cadherin. Blocking this cascade with inhibitors of ARF6 enhances VE-cadherin deposition at cell junctions and reduces vascular leak in both tissue culture assays and in live animal models. This blockade prevents pathology in murine collagen-induced arthritis and lethal endotoxemia assays without blocking inflammatory cytokine production. Collectively, these results implicate vascular leak as a key driver of disease pathology and it identifies ARNO/ARF6 as a therapeutic target for the prevention of inflammatory pathologies.

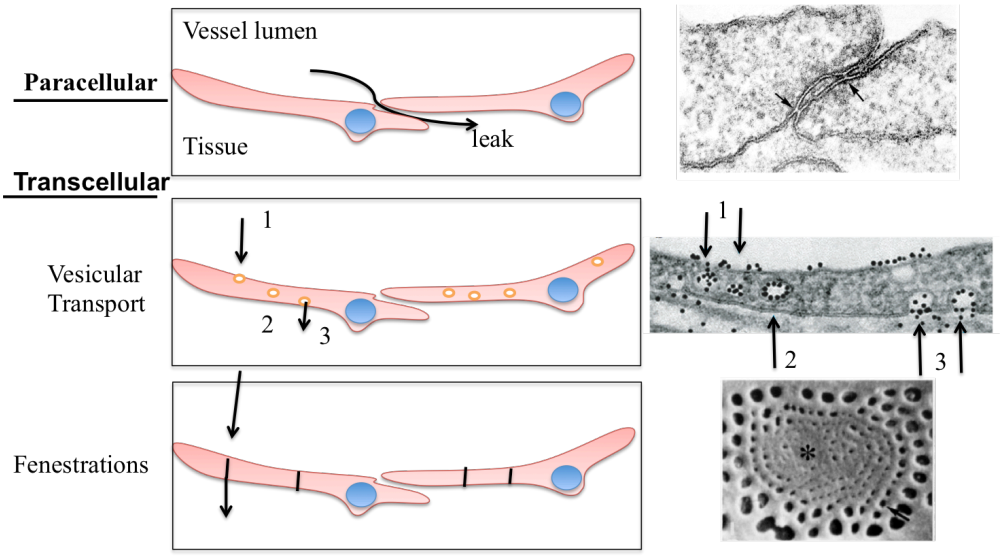

Figure 1.1 **The three mechanisms of vascular leak.** In paracellular vascular leak, luminal components may exit between adjacent endothelial cells through cell junctions. During transcellular vascular leak, (1) luminal components are endocytosed into vesicles, (2) the endocytic vesicle is trafficked to the ablumenal side of the endothelial cell, and (3) the vesicle fuses with the plasma membrane to release the vesicle contents into the peripheral tissues. Fluid may also pass through endothelial fenestrations present in the endothelium of specialized tissues.

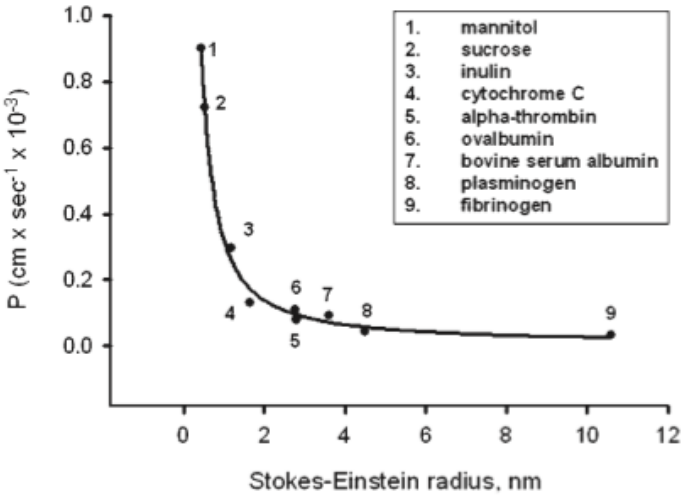

Figure 1.2. **The permeability (P) of various molecules arranged by size through an endothelial monolayer.** Signaling Mechanisms Regulating Endothelial Permeability Dolly Mehta, Asrar B. Malik Physiological Reviews Published 1 January 2006, Vol. 86,. 279-367,DOI: 10.1152/physrev.00012.2005 [6].

References

1. (a) Angus, D.; van der Poll, T., Severe sepsis and septic shock. *The New England journal of medicine* **2013,** *369* (9), 840-51; (b) Weis, S. M., Vascular permeability in cardiovascular disease and cancer. *Current Opinion in Hematology* **2008,** *15* (3), 243-249 10.1097/MOH.0b013e3282f97d86; (c) Chodobski, A.; Zink, B. J.; Szmydynger-Chodobska, J., Blood-brain barrier pathophysiology in traumatic brain injury. *Translational stroke research 2* (4), 492; (d) van Vliet, E. A.; da Costa Araújo, S.; Redeker, S.; van Schaik, R.; Aronica, E.; Gorter, J. A., Blood-brain barrier leakage may lead to progression of temporal lobe epilepsy. *Brain : a journal of neurology* **2007,** *130* (Pt 2), 521-34; (e) Paleolog, E. M., The vasculature in rheumatoid arthritis: cause or consequence? *International journal of experimental pathology* **2009,** *90* (3), 249-61; (f) Minagar, A.; Alexander, J. S., Blood-brain barrier disruption in multiple sclerosis. *Multiple sclerosis (Houndmills, Basingstoke, England)* **2003,** *9* (6), 540-9.

2. Short, K. R.; Kroeze, E. J. B. V.; Fouchier, R. A. M.; Kuiken, T., Pathogenesis of influenza-induced acute respiratory distress syndrome. *The Lancet Infectious Diseases* **2014,** *14* (1), 57-69.

3. Cohen, J., The immunopathogenesis of sepsis. *Nature* **2002,** *420* (6917), 885-91.

4. (a) Annane, D., Corticosteroids for severe sepsis: an evidence-based guide for physicians. *Annals of intensive care* **2011,** *1* (1), 7; (b) Dellinger, R. P.; Levy, M. M.; Rhodes, A.; Annane, D.; Gerlach, H.; Opal, S. M.; Sevransky, J. E.; Sprung, C. L.; Douglas, I. S.; Jaeschke, R.; Osborn, T. M.; Nunnally, M. E.; Townsend, S. R.; Reinhart, K.; Kleinpell, R. M.; Angus, D. C.; Deutschman, C. S.; Machado, F. R.; Rubenfeld, G. D.; Webb, S.; Beale, R. J.; Vincent, J. L.; Moreno, R.; Surviving Sepsis Campaign Guidelines Committee including The Pediatric, S., Surviving Sepsis Campaign: international guidelines for management of severe sepsis and septic shock, 2012. *Intensive care medicine* **2013,** *39* (2), 165-228.

5. Komarova, Y.; Malik, A. B., Regulation of Endothelial Permeability via Paracellular and Transcellular Transport Pathways. *Annual Review of Physiology* **2010,** *72* (1), 463-493.

6. Mehta, D.; Malik, A. B., Signaling mechanisms regulating endothelial permeability. *Physiological reviews* **2006,** *86* (1), 279.

7. Dejana, E.; Tournier-Lasserve, E.; Weinstein, B. M., The control of vascular integrity by endothelial cell junctions: molecular basis and pathological implications. *Developmental cell* **2009,** *16* (2), 209-221.

8. Stockton, R. A.; Schaefer, E.; Schwartz, M. A., p21-activated kinase regulates endothelial permeability through modulation of contractility. *The Journal of biological chemistry* **2004,** *279* (45), 46621-30.

9. Taddei, A.; Giampietro, C.; Conti, A.; Orsenigo, F.; Breviario, F.; Pirazzoli, V.; Potente, M.; Daly, C.; Dimmeler, S.; Dejana, E., Endothelial adherens junctions control tight junctions by VE-cadherin-mediated upregulation of claudin-5. *Nature cell biology* **2008,** *10* (8), 923-34.

10. Vestweber, D.; Winderlich, M.; Cagna, G.; Nottebaum, A., Cell adhesion dynamics at endothelial junctions: VE-cadherin as a major player. *Trends in cell biology* **2009,** *19* (1), 8-15.

11. Cain, R.; Vanhaesebroeck, B.; Ridley, A., The PI3K p110α isoform regulates endothelial adherens junctions via Pyk2 and Rac1. *The Journal of cell biology* **2010,** *188* (6), 863.

12. (a) Rabiet, M.-J.; Plantier, J.-L.; Rival, Y.; Genoux, Y.; Lampugnani, M.-G.; Dejana, E., Thrombin-Induced Increase in Endothelial Permeability Is Associated With Changes in Cell-to-Cell Junction Organization. *Arteriosclerosis, Thrombosis, and Vascular Biology* **1996,** *16* (3), 488-496; (b) Gavard, J.; Gutkind, J. S., VEGF controls endothelial-cell permeability by promoting the beta-arrestin-dependent endocytosis of VE-cadherin. *Nature cell biology* **2006,** *8* (11), 1223-34.

13. Gavard, J.; Patel, V.; Gutkind, J. S., Angiopoietin-1 prevents VEGF-induced endothelial permeability by sequestering Src through mDia. *Developmental cell* **2008,** *14* (1), 25-36.

14. London, N. R.; Zhu, W.; Bozza, F. A.; Smith, M. C. P.; Greif, D. M.; Sorensen, L. K.; Chen, L.; Kaminoh, Y.; Chan, A. C.; Passi, S. F.; Day, C. W.; Barnard, D. L.; Zimmerman, G. A.; Krasnow, M. A.; Li, D. Y., Targeting Robo4-Dependent Slit Signaling to Survive the Cytokine Storm in Sepsis and Influenza. *Science Translational Medicine* **2010,** *2* (23), 23ra19-23ra19.

15. Jones, C.; Nishiya, N.; London, N.; Zhu, W.; Sorensen, L.; Chan, A.; Lim, C.; Chen, H.; Zhang, Q.; Schultz, P.; Hayallah, I.; Thomas, K.; Famulok, M.; Zhang, K.; Ginsberg, M.; Li, D., Slit2–Robo4 signalling promotes vascular stability by blocking Arf6 activity. *Nature cell biology* **2009**.

16. Donaldson, J. G.; Honda, A., Localization and function of Arf family GTPases. *Biochemical Society transactions* **2005,** *33* (Pt 4), 639-42.

17. Donaldson, J. G.; Jackson, C. L., ARF family G proteins and their regulators: roles in membrane transport, development and disease. *Nature Reviews Molecular Cell Biology* **2011,** *12* (6), 362-375.

18. Honda, A.; Nogami, M.; Yokozeki, T.; Yamazaki, M.; Nakamura, H.; Watanabe, H.; Kawamoto, K.; Nakayama, K.; Morris, A. J.; Frohman, M. A.; Kanaho, Y., Phosphatidylinositol 4-phosphate 5-kinase alpha is a downstream effector of the small G protein ARF6 in membrane ruffle formation. *Cell* **1999,** *99* (5), 521-32.

19. Morishige, M.; Hashimoto, S.; Ogawa, E.; Toda, Y.; Kotani, H.; Hirose, M.; Wei, S.; Hashimoto, A.; Yamada, A.; Yano, H.; Mazaki, Y.; Kodama, H.; Nio, Y.; Manabe, T.; Wada, H.; Kobayashi, H.; Sabe, H., GEP100 links epidermal growth factor receptor signalling to Arf6 activation to induce breast cancer invasion. *Nature cell biology* **2008,** *10* (1), 85-92.

20. Hashimoto, A.; Hashimoto, S.; Ando, R.; Noda, K.; Ogawa, E.; Kotani, H.; Hirose, M.; Menju, T.; Morishige, M.; Manabe, T.; Toda, Y.; Ishida, S.; Sabe, H., GEP100-Arf6-AMAP1-Cortactin Pathway Frequently Used in Cancer Invasion Is Activated by VEGFR2 to Promote Angiogenesis. *PLoS One* **2011,** *6* (8).

21. Hafner, M.; Schmitz, A.; Gr|[Uuml]|Ne, I.; Srivatsan, S. G.; Paul, B.; Kolanus, W.; Quast, T.; Kremmer, E.; Bauer, I.; Famulok, M., Inhibition of cytohesins by SecinH3 leads to hepatic insulin resistance. *Nature* **2006,** *444* (7121), 941.

22. (a) Pober, J. S.; Sessa, W. C., Evolving functions of endothelial cells in inflammation. *Nature Reviews Immunology* **2007,** *7* (10), 803; (b) Tracey, K. J.; Fong, Y.; Hesse, D. G.; Manogue, K. R.; Lee, A. T.; Kuo, G. C.; Lowry, S. F.; Cerami, A., Anti-cachectin/TNF monoclonal antibodies prevent septic shock during lethal bacteraemia. *Nature* **1987,** *330* (6149), 662-4; (c) Reinhart, K.; Karzai, W., Anti-tumor necrosis factor therapy in sepsis: update on clinical trials and lessons learned. *Critical care medicine* **2001,** *29* (7 Suppl), S121-5.

23. McInnes, I. B.; Schett, G., Cytokines in the pathogenesis of rheumatoid arthritis. *Nature Reviews Immunology* **2007,** *7* (6), 429-42.

24. Riedemann, N. C.; Guo, R. F.; Ward, P. A., Novel strategies for the treatment of sepsis. *Nature medicine* **2003,** *9* (5), 517-24.

25. (a) Opal, S.; Laterre, P. F.; Francois, B.; LaRosa, S. P.; Angus, D.; Mira, J. P.; Wittebole, X.; Dugernier, T.; Perrotin, D.; Tidswell, M.; Jauregui, L.; Krell, K.; Pachl, J.; Takahashi, T.; Peckelsen, C.; Cordasco, E.; Chang, C. S.; Oeyen, S.; Aikawa, N.; Maruyama, T.; Schein, R.; Kalil, A. C.; Van Nuffelen, M.; Lynn, M.; Rossignol, D. P.; Gogate, J.; Roberts, M. B.; Wheeler, J. L.; Vincent, J.; Group, A. S., Effect of eritoran, an antagonist of MD2-TLR4, on mortality in patients with severe sepsis: the ACCESS randomized trial. *JAMA* **2013,** *309* (11), 1154-62; (b) Da Silva, J. A.; Jacobs, J. W.; Kirwan, J. R.; Boers, M.; Saag, K. G.; Inês, L. B.; de Koning, E. J.; Buttgereit, F.; Cutolo, M.; Capell, H.; Rau, R.; Bijlsma, J. W., Safety of low dose glucocorticoid treatment in rheumatoid arthritis: published evidence and prospective trial data. *Annals of the rheumatic diseases* **2006,** *65* (3), 285-93; (c) Connor, V., Anti-TNF therapies: a comprehensive analysis of adverse effects associated with immunosuppression. *Rheumatology International* **2011,** *31* (3), 327-337.

CHAPTER 2

INTERLEUKIN RECEPTOR ACTIVATES A MYD88-ARNO-ARF6 CASCADE TO DISRUPT VASCULAR STABILITY

The following chapter was reprinted with permission from Macmillian Publishers Limited. My co-authors were Weiquan Zhu, Nyall London, Christopher Gibson, Zongzhong Tong, Lise K. Sorensen, Dallas S. Shi, Jinping Guo, Matthew C.P. Smith, Allie H. Grossmann, Kirk R. Thomas, and Dean Y. Li. This article was originally published in Nature, 2012 Dec; 492:252-255. Here we identify the MYD88-ARNO-ARF6 cascade and illustrate how IL-1β utilizes it to induce endothelial permeability.

LETTER

doi:10.1038/nature11603

Interleukin receptor activates a MYD88–ARNO–ARF6 cascade to disrupt vascular stability

Weiquan Zhu[1,2]*, Nyall R. London[1,2,3]*, Christopher C. Gibson[2,4]*, Chadwick T. Davis[2,5], Zongzhong Tong[6], Lise K. Sorensen[2], Dallas S. Shi[2,5], Jinping Guo[1,2,7], Matthew C. P. Smith[1,2,3], Allie H. Grossmann[2,8], Kirk R. Thomas[1,2] & Dean Y. Li[1,2,3,9,10]

The innate immune response is essential for combating infectious disease. Macrophages and other cells respond to infection by releasing cytokines, such as interleukin-1β (IL-1β), which in turn activate a well-described, myeloid-differentiation factor 88 (MYD88)-mediated, nuclear factor-κB (NF-κB)-dependent transcriptional pathway that results in inflammatory-cell activation and recruitment[1–4]. Endothelial cells, which usually serve as a barrier to the movement of inflammatory cells out of the blood and into tissue, are also critical mediators of the inflammatory response[5,6]. Paradoxically, the cytokines vital to a successful immune defence also have disruptive effects on endothelial cell–cell interactions and can trigger degradation of barrier function and dissociation of tissue architecture[7–9]. The mechanism of this barrier dissolution and its relationship to the canonical NF-κB pathway remain poorly defined. Here we show that the direct, immediate and disruptive effects of IL-1β on endothelial stability in a human *in vitro* cell model are NF-κB independent and are instead the result of signalling through the small GTPase ADP-ribosylation factor 6 (ARF6) and its activator ARF nucleotide binding site opener (ARNO; also known as CYTH2). Moreover, we show that ARNO binds directly to the adaptor protein MYD88, and thus propose MYD88–ARNO–ARF6 as a proximal IL-1β signalling pathway distinct from that mediated by NF-κB. Finally, we show that SecinH3, an inhibitor of ARF guanine nucleotide-exchange factors such as ARNO, enhances vascular stability and significantly improves outcomes in animal models of inflammatory arthritis and acute inflammation.

A defining characteristic of the cytokine-induced inflammatory response is the destabilization of endothelial barriers resulting in vascular permeability[7–9]. To dissect the pathway(s) involved in this tissue disruption, we treated cultured monolayers of human dermal microvascular endothelial cells (HMVEC-d) with IL-1β, and detected an increase in endothelial permeability within 15 min (Fig. 1a). The canonical IL-1β pathway involves ligand-stimulated activation of interleukin-1 receptor (IL-1R), which recruits MYD88 to its cytoplasmic tail[10]. The subsequent signalling cascade through IRAK1 results in the phosphorylation of IκB-α by the IκB kinase (IKK) complex, leading to translocation of NF-κB to the nucleus and the eventual transcription of target genes that promote inflammatory-cell responses[3,4] (Supplementary Fig. 1). To test the involvement of this pathway in IL-1β-induced vascular permeability, cells were treated with the IKK inhibitor SC-514 (ref. 11). Although SC-514 prevented IL-1β-induced nuclear localization of NF-κB, it was unable to rescue either IL-1β-induced permeability or disruption of vascular endothelial (VE)-cadherin surface localization (Fig. 1b, c and Supplementary Fig. 2a–c). We also wondered whether IL-1β-induced vascular permeability required other known MYD88-mediated downstream signalling mechanisms, including ERK1/2, p38 and JNK (also known as MAPK3/MAPK1, MAPK14 and MAPK8, respectively)[12,13]. Although ERK1/2, p38 and JNK were activated by IL-1β stimulation of endothelial cells, small-molecule inhibitors of each of these pathways were unable to prevent IL-1β-induced vascular permeability or IL-1β-induced disruption of VE-cadherin cell-surface localization (Supplementary Fig. 2d–h). Although specific NF-κB targets, such as VEGFA, COX-2 (also known as PTGS2) and the COX-2 product prostaglandin E_2 are modulated by IL-1β, their activation had no effect on IL-1β-induced endothelial permeability[3,14,15] (Supplementary Fig. 3a–e). Finally, treatment with actinomycin D or cycloheximide effectively inhibited transcription or translation, respectively, of NF-κB targets, but did not blunt IL-1β-induced permeability (Fig. 1d and Supplementary Fig. 3f, g). These data strongly support a role for the immediate and destabilizing effects of IL-1β on endothelial stability through signalling pathways independent of NF-κB, transcription and translation.

IL-1β can disrupt VE-cadherin cell-surface localization by promoting endocytic internalization[9]. We proposed that IL-1β might use ARF6, a known regulator of adherens protein localization[16,17]. Indeed, IL-1β activated ARF6 in HMVEC-d within 1 min, a response accompanied by increased endocytosis of VE-cadherin within 5 min and an increase in monolayer permeability within 15 min (Fig. 1a, e and Supplementary Fig. 4a, b). IL-1β treatment did not affect total VE-cadherin messenger RNA or protein levels (Supplementary Fig. 4c, d). Adenoviral-mediated overexpression of constitutively active ARF6 (ARF6(Q67L))[18] elicited a dose-dependent increase in endothelial permeability, as well as a disruption of VE-cadherin cell-surface localization (Fig. 1f, g and Supplementary Fig. 4e, f). A similar dose-dependent loss of total VE-cadherin was also observed, probably through internalization and subsequent degradation (Supplementary Fig. 4g). Interestingly, at lower doses of adenovirus at which permeability was still induced, loss of total VE-cadherin was not observed, but a dose-dependent loss of cell-surface VE-cadherin occurred (Fig. 1f–h and Supplementary Fig. 4g). Moreover, short interfering RNA (siRNA) knockdown of *ARF6* enhanced VE-cadherin cell-surface localization and prevented both IL-1β-induced disruption of VE-cadherin and IL-1β-induced endothelial permeability (Fig. 1i–k and Supplementary Fig. 4h, i). Collectively, these data link ARF6 as a critical regulator of VE-cadherin trafficking by controlling cell-surface localization and the immediate and disruptive effects of IL-1β-induced vascular permeability.

The ARF6 activation state is decreased through interaction with GTPase-activating proteins (GAPs) and increased through interaction with guanine nucleotide-exchange factors (GEFs). Consistent with this, treatment of endothelial cells with the ARF-GAP inhibitor QS11 evoked an increase in ARF6–GTP, a decrease in VE-cadherin cell-surface localization and increased permeability (Fig. 2a–d and

[1]Department of Medicine, University of Utah, Salt Lake City, Utah 84112, USA. [2]Program in Molecular Medicine, University of Utah, Salt Lake City, Utah 84112, USA. [3]Department of Oncological Sciences, University of Utah, Salt Lake City, Utah 84112, USA. [4]Department of Bioengineering, University of Utah, Salt Lake City, Utah 84112, USA. [5]Department of Human Genetics, University of Utah, Salt Lake City, Utah 84112, USA. [6]Navigen Inc, Salt Lake City, Utah 84112, USA. [7]Department of Anatomy, Second Military Medical University, Shanghai 200433, China. [8]Department of Pathology, University of Utah, Salt Lake City, Utah 84112, USA. [9]Cardiology Section, VA Salt Lake City Health Care System, Salt Lake City, Utah 84112, USA. [10]The Key Laboratory for Human Disease Gene Study of Sichuan Province, Institute of Laboratory Medicine, Sichuan Academy of Medical Sciences & Sichuan Provincial People's Hospital, Chengdu, Sichuan 610072, China.
*These authors contributed equally to this work.

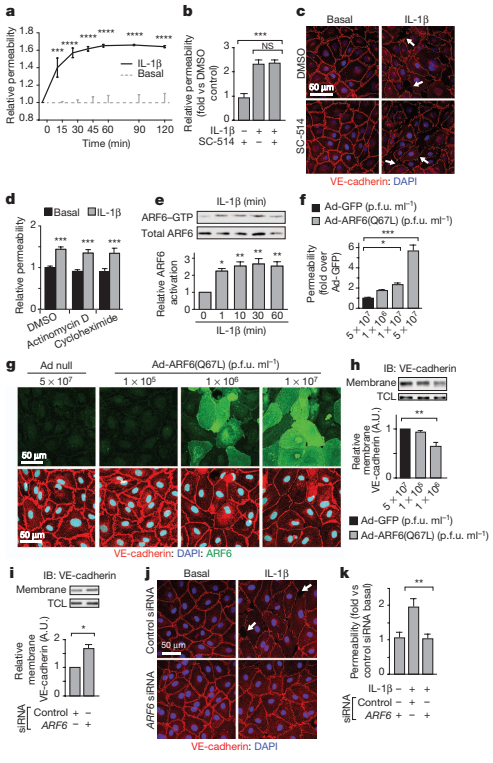

Figure 1 | Immediate effects of IL-1β are NF-κB independent and ARF6 dependent. a–d, Monolayers of HMVEC-d stimulated with IL-1β and assayed for permeability to horseradish peroxidase (HRP) over time (**a**), permeability to HRP following 2-h treatment with SC-514 (**b**), immunofluorescent localization of VE-cadherin (**c**) and permeability to HRP after 30-min treatment with actinomycin D or cycloheximide (**d**). **e**, IL-1β-stimulated HMVEC-d lysates were precipitated with glutathione *S*-transferase (GST)–GGA3 and immunoblotted for ARF6. **f–i**, HMVEC-d monolayers infected with adenovirus (Ad) containing empty vector (null), green fluorescent protein (GFP) or ARF6(Q67L), showing permeability (**f**) and VE-cadherin localization (**g**) (green denotes ARF6 expression). Membrane fractions from adenoviral-vector-infected (**h**) or *ARF6*-siRNA-treated (**i**) HMVEC-d were immunoblotted for VE-cadherin. **j**, **k**, *ARF6*-siRNA-treated HMVEC-d stimulated with IL-1β, showing VE-cadherin localization (**j**) (arrows denote disrupted VE-cadherin cell-surface localization) and permeability (**k**). A.U., arbitrary unit; DMSO, dimethylsulphoxide; IB, immunoblot; TCL, total cell lysate. $n \geq 3$; error bars denote s.e.m. $^{*}P < 0.05$, $^{**}P < 0.01$, $^{***}P < 0.001$, $^{****}P < 0.0001$.

Supplementary Fig. 5a, b)[19]. We noted that a class of ARF-GEFs, the cytohesins, is highly expressed in multiple types of endothelial cells (Supplementary Fig. 5c). Accordingly, treatment of HMVEC-d with SecinH3, a cytohesin inhibitor, significantly increased endothelial cell-surface localization of VE-cadherin (Supplementary Fig. 5d–f)[20]. Notably, SecinH3 inhibited IL-1β-induced ARF6–GTP, as well as IL-1β-induced disruption of VE-cadherin cell-surface localization and endothelial permeability (Fig. 2e–g and Supplementary Fig. 5g, h). To determine which GEF might be uniquely involved, we used siRNA to knockdown *CYTH1*, *ARNO* and *CYTH3* (coding for cytohesins 1, 2 and 3, respectively) and *GEP100* (also known as *IQSEC1*) (Supplementary Fig. 6a), and found that only siRNA targeting *ARNO* completely blocked IL-1β-induced endothelial permeability and phenocopied the knockdown of *ARF6* (Fig. 2h and Supplementary Fig. 6b). Furthermore, *ARNO* siRNA inhibited IL-1β-induced ARF6–GTP formation, IL-1β-induced disruption of VE-cadherin cell–cell contacts and IL-1β-induced internalization of surface VE-cadherin (Fig. 2i, j and Supplementary Fig. 6c, g); all of these effects were rescued by the expression of siRNA-resistant *ARNO* (Supplementary Fig. 6d–g). In cells treated with *ARNO* siRNA, viral expression of siRNA-resistant *ARNO*, but not viral expression of siRNA-resistant *ARNO(E156K)* (carrying a mutation in the Sec7 domain), rescued the disruption of IL-1β-induced ARF6–GTP formation and permeability[21] (Supplementary Fig. 6d, e). These data demonstrate that ARNO is a critical ARF-GEF necessary for IL-1β-induced activation of ARF6 and subsequent induction of vascular permeability, but does not rule out the role of other GEF family members in similar responses in different cell types or in response to different cytokines.

The signalling components in the NF-κB pathway downstream of IL-1β-induced activation of IL-1R are well characterized (Supplementary Fig. 1). Although the inhibition of the NF-κB pathway at the level of IRAK1 by siRNA did not inhibit IL-1β-induced ARF6 activation, siRNA knockdown of *MYD88* inhibited both IL-1β-induced permeability and ARF6–GTP activation, suggesting a bifurcation of

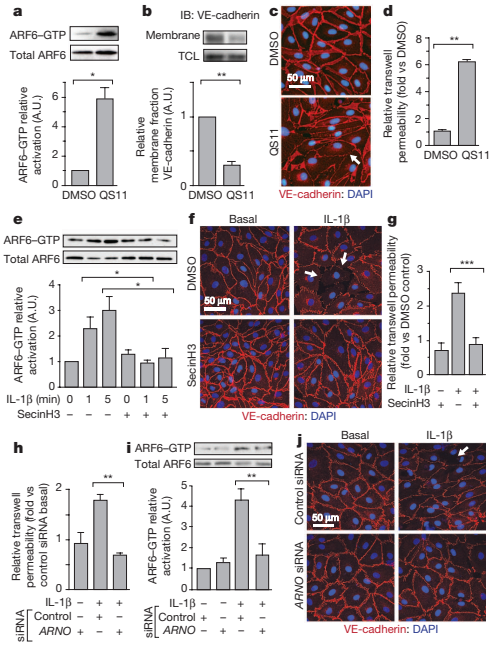

Figure 2 | Inhibition of ARF-GAPs and ARF-GEFs affect ARF6 activation and VE-cadherin localization. a–d, HMVEC-d treated with QS11, showing whole-cell lysates precipitated with GST–GGA3 and immunoblotted for ARF6 (**a**), membrane fractions immunoblotted for VE-cadherin (**b**), immunofluorescence for VE-cadherin (red) (**c**) and permeability to HRP (**d**). **e–g**, HMVEC-d treated with IL-1β and SecinH3, showing immunoblotting for ARF6 (**e**), immunofluorescence for VE-cadherin (**f**) and permeability to HRP (**g**). **h–j**, HMVEC-d treated with anti-*ARNO* siRNA and stimulated with IL-1β, showing permeability to HRP (**h**), GST–GGA3 precipitation and ARF6 immunoblotting (**i**) and immunofluorescence of VE-cadherin (**j**). Arrow denotes less cell-surface VE-cadherin. $n \geq 3$; error bars denote s.e.m. $^{*}P < 0.05$, $^{**}P < 0.01$, $^{***}P < 0.001$.

IL-1β-induced signalling at the point of MYD88 (Fig. 3a–c and Supplementary Fig. 7a, b). The proposed bifurcation was further verified by the pharmacological uncoupling of the two pathway arms: although SecinH3 blunted IL-1β-induced permeability, it did not significantly inhibit IL-1β-induced NF-κB nuclear localization or NF-κB-dependent expression or localization of cell-surface adhesion molecules (Fig. 3d and Supplementary Fig. 7c, d). Furthermore, SecinH3 was unable to inhibit IL-1β-induced polymorphonuclear leukocyte rolling and adherence under shear stress on an endothelial monolayer (Supplementary Fig. 7e). Mechanistic support for this novel signalling arm was provided by the demonstration of an interaction between MYD88 and ARNO by co-immunoprecipitation in both overexpression and endogenous settings (Fig. 3e, f). Our hypothesis that ARNO is the critical GEF in IL-1β-induced permeability in endothelial cells was further strengthened by our inability to detect an interaction between MYD88 and other potentially relevant ARF-GEFs including CYTH1, CYTH3 and GEP100 (Supplementary Fig. 7f, g).

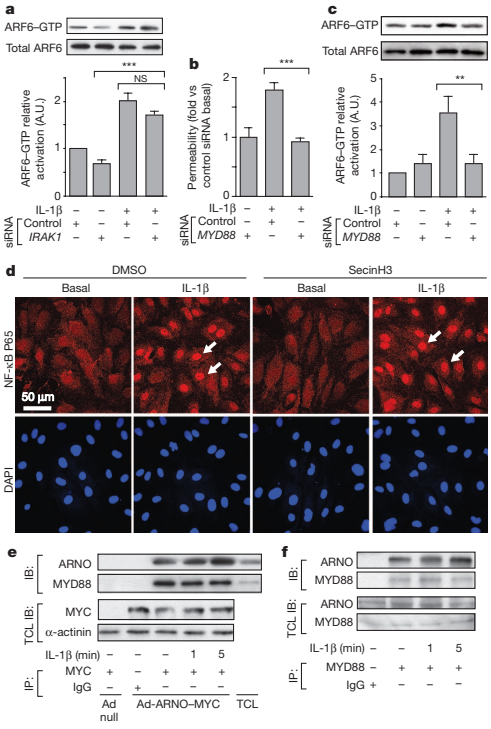

Figure 3 | The immediate IL-1β-induced permeability pathway diverges at MYD88. **a**, *IRAK1*-siRNA-treated HMVEC-d, stimulated with IL-1β, subjected to ARF6–GTP pull-down and immunoblotted for ARF6. **b**, **c**, *MYD88*-siRNA-treated HMVEC-d stimulated with IL-1β, showing permeability and ARF6 activation. **d**, NF-κB p65 (also known as RELA) immunofluorescence in HMVEC-d stimulated with IL-1β and SecinH3. Arrows denote nuclear localization. **e**, Cell lysates from Ad-ARNO–MYC-infected HMVEC-d immunoprecipitated (IP) with anti-MYC antibodies and immunoblotted with anti-MYD88 antibodies. **f**, Lysates from HMVEC-d immunoprecipitated with anti-MYD88 antibodies and immunoblotted with anti-ARNO antibodies. $n \geq 3$. Error bars denote s.e.m. $^{*}P < 0.05$, $^{**}P < 0.01$, $^{***}P < 0.001$.

An effective therapeutic strategy to combat numerous inflammatory conditions is to target pro-inflammatory cytokines proximal to the NF-κB pathway. However, this strategy can result in undesired pleiotropic effects. We wanted to know whether targeting a single arm in this pathway—the one mediated by ARNO–ARF6—could inhibit acute or chronic inflammation *in vivo* in two animal models of inflammation. The first model we tested was rheumatoid arthritis, a disease characterized by a dysregulated cytokine response causing excessive inflammation and tissue damage and treated therapeutically in humans with the anti-cytokine tumour necrosis factor receptor (TNFR)–Fc fusion protein etanercept (Enbrel)[22–25]. A standard animal model of arthritis through which a TNFR fusion approach has been proven effective is collagen-induced arthritis (CIA)[24–26]. Exposure of animals to the cytohesin inhibitor SecinH3 after the onset of CIA reduced vascular permeability in the joints, but had no effect on global cytokine levels at 24 h after treatment initiation (Fig. 4a and Supplementary Fig. 8a, b). In addition, a significant inhibition in the increase in arthritic index, comparable to that achieved by treatment with Enbrel, was observed. The arthritic index is a scoring system determined by the number of digits or joints that are oedematous or erythematous. The significance of our findings was verified by histologic scoring of inflammation, pannus development, cartilage damage and bone damage (Fig. 4c, d). A similar effect of SecinH3 was confirmed in a second model of inflammation, the carrageenan air-pouch model. Six hours after an inflammatory stimulus, a time at which substantial inflammation was induced in the positive control mice, treatment with SecinH3 decreased exudate volume as well as leukocyte concentration in the exudates (Supplementary Fig. 8c, d). Collectively, these data identify MYD88–ARNO–ARF6 as a valid target for inflammatory conditions confirming a relevant role for manipulation of this pathway *in vivo* to modulate inflammatory processes and in the treatment of disease.

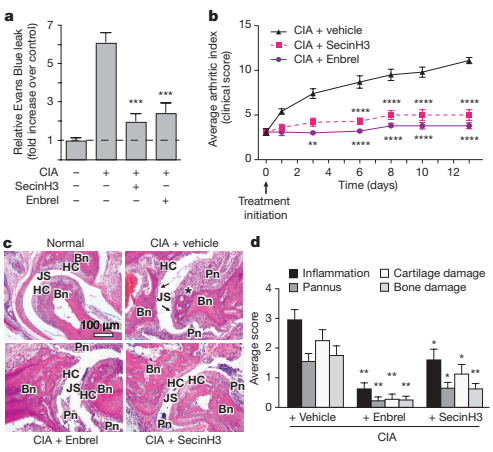

Figure 4 | Inhibition of ARF-GEFs decreases collagen-induced vascular permeability and arthritis in mice. **a**, Arthritis-induced vascular permeability in the joint measured by Evans Blue leak 7 days after treatment initiation in the presence of SecinH3 or Enbrel. $n = 14$ per group. **b**, Chronological arthritic assessment. $n = 10$ per group. Significance values are measured against CIA plus vehicle. **c**, Haematoxylin and eosin staining of sections through joints. Bn, bone; HC; hyaline cartilage; JS, joint space; Pn, inflamed pannus. Asterisk denotes cartilage and bone loss; arrows denote eroded cartilage. **d**, Summary of histological changes of inflammation, pannus, cartilage and bone damage of indicated treatment. Control, $n = 5$; Enbrel and SecinH3, $n = 10$. Error bars denote s.e.m. $^{*}P < 0.05$, $^{**}P < 0.01$, $^{***}P < 0.001$, $^{****}P < 0.0001$ versus disease group.

Chronic inflammation causes tissue destruction through dysregulated cytokine release, inflammatory cell recruitment and vascular permeability; yet each of these mechanisms has critical roles in many physiologic processes, including the immune response[5,7]. We have identified a novel pathway that uncouples cytokine effects on vascular stability from other critical functions of the canonical NF-κB transcription program (Supplementary Fig. 1). Our model suggests the potential for inhibition of vascular leak without modulation of immune-cell adhesion or other critical NF-κB-dependent responses.

The activation of many inflammatory cytokine receptors disrupts cell–cell interactions, precipitating tissue oedema and destruction[5,7,9,27]. Toll-like receptors and the interleukin receptor also use MYD88, and the mechanism described here may well apply[3,10]. Interestingly, TNFR1 (also known as TNFRSF1A) does not use MYD88 yet still activates ARF6–GTP after stimulation (Supplementary Fig. 9). Whether ARNO or another ARF-GEF binds directly to TNFR1 or its adaptor protein TRADD is unknown, as is the possibility that ARF-GEF–ARF6–cadherin serves as a common signalling module exploited by multiple cytokines. Although this study focused on the endothelium, the concept of cytokine receptor–ARF–cadherin may also apply to the epithelial barrier, which expresses these constituents and is also compromised by cytokines including IL-1β[16].

Inhibition of this novel vascular-stability pathway, which is aimed at enhancing the resilience of the host to the cytokine response, shows effects commensurate to those of class-leading drugs that target cytokines upstream of NF-κB and seek to blunt the cytokine response of the immune system outright. This approach may be particularly useful in arthritis, as the current medical therapy can render a patient immunocompromised and susceptible to reactivation of infectious disease such as tuberculosis[28]. Application of these findings to other diseases characterized by excessive acute or chronic inflammatory states, including sepsis, Crohn's disease, ulcerative colitis, scleroderma and psoriasis, should also be considered[9,29,30].

METHODS SUMMARY

Transwell permeability. HMVEC-d cells were seeded on 1.0-μm Costar transwell inserts coated with fibronectin. Cells were grown to confluency and treated with SecinH3 for 3 h or MAPK/NF-κB/transcription/translation inhibitors for 30 min followed by treatment with 10 ng ml^{-1} IL-1β. Alternatively, cells were infected with Ad-GFP or Ad-ARF6(Q67L) for 48 h. siRNA knockdown was performed as described in Supplementary Methods, and cells were treated with IL-1β 72 h after the second siRNA transfection. Two hours later, HRP was added to the top chamber at a final concentration of 100 μg ml^{-1}. Medium was removed after 60 min from the lower chamber. For time-course transwell assays and transcription/translation-inhibitor experiments (Fig. 1a, c, d), HRP was added to the insert at the same time as IL-1β. Transwell inserts were moved to fresh wells after each time point, and the concentration of HRP in the bottom chamber was measured for monolayer permeability. HRP was assessed using media samples obtained from the lower chamber incubated with 0.5 mM of guaiacol and 0.6 mM H_2O_2. Spectrophotometric analysis of absorbance at 490 nm provided a quantitative evaluation of the amount of HRP that crossed the membrane. Data are presented as mean ± s.e.m. of at least three independent experiments performed in quadruplicate.

A detailed description of all methods is provided in Supplementary Information.

Received 9 December 2011; accepted 19 September 2012.
Published online 11 November 2012.

1. Li, Q. & Verma, I. M. NF-κB regulation in the immune system. *Nature Rev. Immunol.* **2,** 725–734 (2002).
2. Collins, T. *et al.* Transcriptional regulation of endothelial cell adhesion molecules: NF-κB and cytokine-inducible enhancers. *FASEB J.* **9,** 899–909 (1995).
3. Liu, S. F. & Malik, A. B. NF-κB activation as a pathological mechanism of septic shock and inflammation. *Am. J. Physiol. Lung Cell. Mol. Physiol.* **290,** L622–L645 (2006).
4. Rothwarf, D. M. & Karin, M. The NF-κB activation pathway: a paradigm in information transfer from membrane to nucleus. *Sci. STKE* **1999,** RE1 (1999).
5. Pober, J. S. & Sessa, W. C. Evolving functions of endothelial cells in inflammation. *Nature Rev. Immunol.* **7,** 803–815 (2007).
6. Muller, W. A. Leukocyte–endothelial cell interactions in the inflammatory response. *Lab. Invest.* **82,** 521–533 (2002).
7. Royall, J. A. *et al.* Tumor necrosis factor and interleukin 1 alpha increase vascular endothelial permeability. *Am. J. Physiol. Lung Cell. Mol. Physiol.* **257,** L399–L410 (1989).
8. West, X. Z. *et al.* Oxidative stress induces angiogenesis by activating TLR2 with novel endogenous ligands. *Nature* **467,** 972–976 (2010).
9. London, N. R. *et al.* Targeting Robo4-dependent Slit signaling to survive the cytokine storm in sepsis and influenza. *Sci. Transl. Med.* **2,** 23ra19 (2010).
10. Zhu, J. & Mohan, C. Toll-like receptor signaling pathways–therapeutic opportunities. *Mediators Inflamm.* **2010,** 781235 (2010).
11. Kishore, N. *et al.* A selective IKK-2 inhibitor blocks NF-κB-dependent gene expression in interleukin-1β-stimulated synovial fibroblasts. *J. Biol. Chem.* **278,** 32861–32871 (2003).
12. Matthews, J. S. & O'Neill, L. A. Distinct roles for p42/p44 and p38 mitogen-activated protein kinases in the induction of IL-2 by IL-1. *Cytokine* **11,** 643–655 (1999).
13. Martin, M. U. & Wesche, H. Summary and comparison of the signaling mechanisms of the Toll/interleukin-1 receptor family. *Biochim. Biophys. Acta* **1592,** 265–280 (2002).
14. Kaltschmidt, B., Linker, R. A., Deng, J. & Kaltschmidt, C. Cyclooxygenase-2 is a neuronal target gene of NF-κB. *BMC Mol. Biol.* **3,** 16 (2002).
15. Funk, C. D. Prostaglandins and leukotrienes: advances in eicosanoid biology. *Science* **294,** 1871–1875 (2001).
16. Palacios, F., Price, L., Schweitzer, J., Collard, J. G. & D'Souza-Schorey, C. An essential role for ARF6-regulated membrane traffic in adherens junction turnover and epithelial cell migration. *EMBO J.* **20,** 4973–4986 (2001).
17. D'Souza-Schorey, C., Li, G., Colombo, M. I. & Stahl, P. D. A regulatory role for ARF6 in receptor-mediated endocytosis. *Science* **267,** 1175–1178 (1995).
18. Riley, K. N., Maldonado, A. E., Tellier, P., D'Souza-Schorey, C. & Herman, I. M. Betacap73–ARF6 interactions modulate cell shape and motility after injury *in vitro*. *Mol. Biol. Cell* **14,** 4155–4161 (2003).
19. Zhang, Q. *et al.* Small-molecule synergist of the Wnt/β-catenin signaling pathway. *Proc. Natl Acad. Sci. USA* **104,** 7444–7448 (2007).
20. Hafner, M. *et al.* Inhibition of cytohesins by SecinH3 leads to hepatic insulin resistance. *Nature* **444,** 941–944 (2006).
21. Béraud-Dufour, S. *et al.* A glutamic finger in the guanine nucleotide exchange factor ARNO displaces $Mg2^+$ and the β-phosphate to destabilize GDP on ARF1. *EMBO J.* **17,** 3651–3659 (1998).
22. Arend, W. P. Cytokine imbalance in the pathogenesis of rheumatoid arthritis: the role of interleukin-1 receptor antagonist. *Semin. Arthritis Rheum.* **30,** 1–6 (2001).
23. Szekanecz, Z. & Koch, A. E. Vascular involvement in rheumatic diseases: 'vascular rheumatology'. *Arthritis Res. Ther.* **10,** 224 (2008).
24. van den Berg, W. B., Joosten, L. A., Helsen, M. & van de Loo, F. A. Amelioration of established murine collagen-induced arthritis with anti-IL-1 treatment. *Clin. Exp. Immunol.* **95,** 237–243 (1994).
25. Joosten, L. A., Helsen, M. M., van de Loo, F. A. & van den Berg, W. B. Anticytokine treatment of established type II collagen-induced arthritis in DBA/1 mice. A comparative study using anti-TNFα, anti-IL-1α/β, and IL-1Ra. *Arthritis Rheum.* **39,** 797–809 (1996).
26. Wooley, P. H., Dutcher, J., Widmer, M. B. & Gillis, S. Influence of a recombinant human soluble tumor necrosis factor receptor FC fusion protein on type II collagen-induced arthritis in mice. *J. Immunol.* **151,** 6602–6607 (1993).
27. London, N. R., Whitehead, K. J. & Li, D. Y. Endogenous endothelial cell signaling systems maintain vascular stability. *Angiogenesis* **12,** 149–158 (2009).
28. Keane, J. *et al.* Tuberculosis associated with infliximab, a tumor necrosis factor α-neutralizing agent. *N. Engl. J. Med.* **345,** 1098–1104 (2001).
29. Lee, W. L. & Slutsky, A. S. Sepsis and endothelial permeability. *N. Engl. J. Med.* **363,** 689–691 (2010).
30. Silva, L. C., Ortigosa, L. C. & Benard, G. Anti-TNF-α agents in the treatment of immune-mediated inflammatory diseases: mechanisms of action and pitfalls. *Immunotherapy* **2,** 817–833 (2010).

Supplementary Information is available in the online version of the paper.

Acknowledgements We thank D. Lim and T. Mleynek for graphical assistance, G. Zimmerman and J. Kaplan for reading the manuscript, S. Odelberg for reading the manuscript and statistical analysis, J. Ling for help with immunostaining, R. Campbell and A. Weyrich for providing primary human blood cells, C. Rodesch and the University of Utah Cell Imaging/Fluorescence Facility as well as the University of Utah Flow Cytometry Facility, and M. P. Revelo for help with pathology. D.Y.L. and his laboratory were funded by grants from the National Heart, Lung, and Blood Institute; Burroughs Wellcome Fund; Juvenile Diabetes Research Foundation; NIAID Rocky Mountain Regional Center of Excellence in Biodefense and Emerging Infectious Disease; the American Asthma Foundation; and the Department of Defense. D.Y.L. is the HA and Edna Benning Endowed Professor of Medicine and Cardiology.

Author Contributions W.Z., N.R.L., C.C.G. and D.Y.L. were responsible for project conceptualization, experimental design, data analysis and manuscript preparation. W.Z., C.C.G., C.T.D., Z.T., L.K.S., D.S.S. and J.G. performed and collected data for *in vitro* experiments. N.R.L. collected data for *in vivo* experiments. C.C.G. developed software techniques for immunofluorescence analysis. M.C.P.S. performed flow cytometry experiments. Z.T. and K.R.T. made constructs and adenoviruses. A.H.G. provided histology and pathology expertise. D.Y.L. was responsible for funding the project.

Author Information Reprints and permissions information is available at www.nature.com/reprints. The authors declare competing financial interests: details are available in the online version of the paper. Readers are welcome to comment on the online version of the paper. Correspondence and requests for materials should be addressed to D.Y.L. (dean.li@u2m2.utah.edu).

SUPPLEMENTARY INFORMATION doi:10.1038/nature11603

Correction notice

Interleukin receptor activates a MYD88–ARNO–ARF6 cascade to disrupt vascular stability

Weiquan Zhu, Nyall R. London, Christopher C. Gibson, Chadwick T. Davis, Zongzhong Tong, Lise K. Sorensen, Dallas S. Shi, Jinping Guo, Matthew C. P. Smith, Allie H. Grossmann, Kirk R. Thomas & Dean Y. Li

Nature doi:10.1038/nature11603 (11 November 2012)

In the version of the Supplementary Information originally posted online, two images in Supplementary Fig. 4a were incorrect. These have been replaced in the new version of the Supplementary Information; see Supplementary Information Table of Contents for details.

SUPPLEMENTARY INFORMATION

doi:10.1038/nature11603

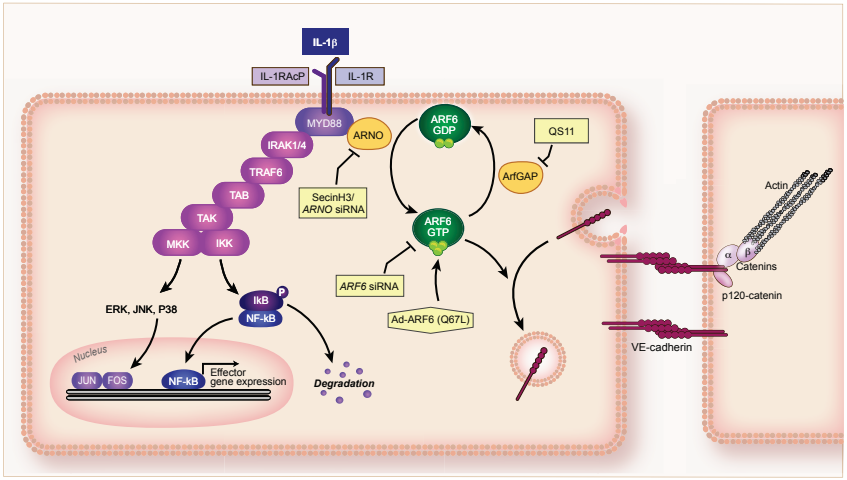

Supplementary Figure 1. Proposed IL-1β signaling pathways.
IL-1β activates NF-κB through a MYD88-IRAK-IκB-dependent pathway. MYD88 also binds to ARNO, and through a divergent pathway enhances ARF6-GTP, and decreases VE-cadherin cell surface localization.

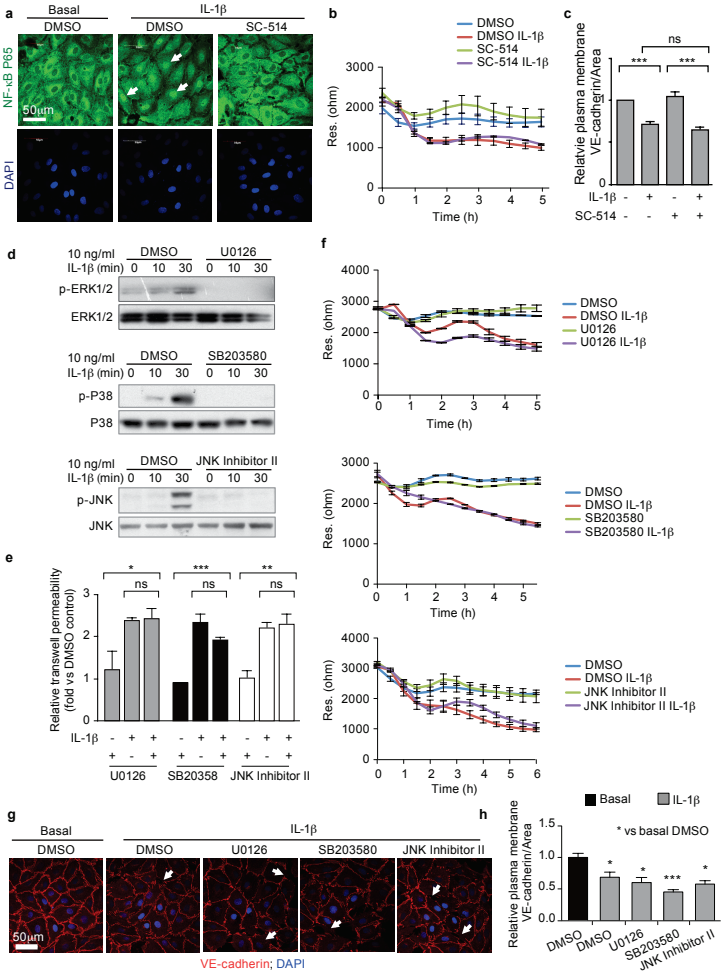

Supplementary Figure 2. IL-1β-induced permeability is independent of NF-κB, ERK1/2, JNK, and p38. **(a)** HMVEC-D cells were stimulated with IL-1β in the presence of DMSO or SC-514 and subjected to immunofluorescence for NF-κB (green). White arrows indicate nuclear NF-κB. **(b)** HMVEC-D cells were stimulated with IL-1β in the presence of DMSO or the NF-κB inhibitor, SC-514. Transendothelial resistance was measured by Electric Cell-substrate Impedance Sensing (ECIS). **(c)** Quantification of IL-1β-induced disruption of plasma membrane VE-cadherin treated with DMSO and SC-514 as shown in Figure 1c. **(d)** Lysates from HMVEC-D cells stimulated with IL-1β in the presence of DMSO, U0126, SB203580 or JNK Inhibitor II were subjected to immunoblotting for p-ERK1/2, p-P38, or p-JNK. **(e)** Transwell permeability of HMVEC-D cells stimulated with IL-1β in the presence of inhibitors of ERK1/2 (U0126), P38 (SB203580), and JNK (JNK Inhibitor II). **(f)** Transendothelial resistance was measured by ECIS in HMVEC-D cells treated with IL-1β in the presence of DMSO, ERK1/2 inhibitor U0126, P38 inhibitor SB203580, or JNK Inhibitor II in EGM2-MV complete media. **(g)** VE-cadherin immunofluorescence of HMVEC-D cells treated with IL-1β in the presence of DMSO, U0126, SB203580, or JNK Inhibitor II. White arrows indicate areas of reduced VE-cadherin surface localization. **(h)** Quantification of (g). For all experiments, N ≥ 3 and error bars represent SEM. * p<0.05, ** p<0.01, *** p<0.001.

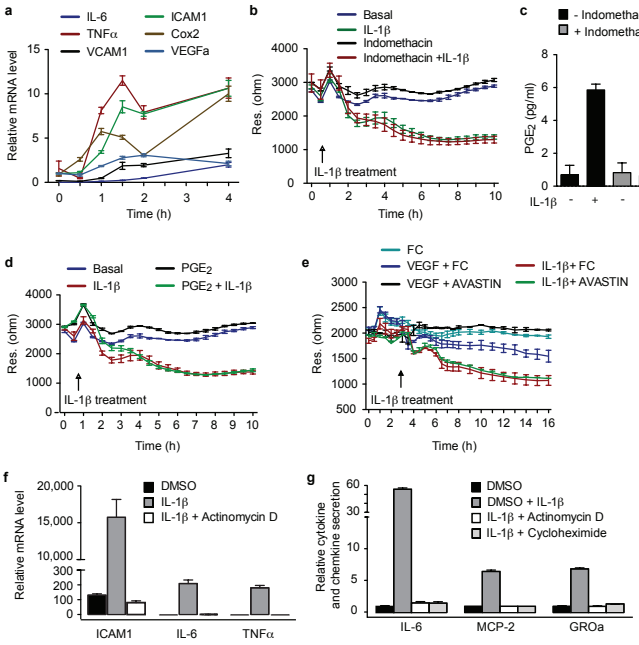

Supplementary Figure 3. IL-1β induced permeability is independent of NF-κB-transcription and its targets. **(a)** HMVEC-D cells treated with IL-1β for 0.5, 1, 1.5, 2 or 4 hours were subjected to quantitative RT-PCR to assess NF-κB target gene mRNA levels. **(b)** Transendothelial resistance was measured by ECIS in HMVEC-D cells treated with IL-1β in the presence or absence of a Cox inhibitor, Indomethacin. **(c)** Conditional media from HMVEC-D cells treated with IL-1β in the presence or absence of Indomethacin were subjected to ELISA for PGE_2. **(d)** Transendothelial resistance was measured by ECIS in HMVEC-D cells treated with IL-1β in the presence of PGE_2. **(e)** Transendothelial resistance was measured by ECIS in HMVEC-D cells treated with IL-1β or VEGF in the presence of anti-VEGF antibody (AVASTIN) or an IgG FC control. **(f)** NF-κB transcriptional targets ICAM1, IL-6 and TNFα mRNA levels were checked by quantitative RT-PCR in HMVEC-D cells treated with IL-1β in the presence or absence of Actinomycin-D. **(g)** NF-κB transcriptional targets IL-6, MCP-2 and GROa protein levels were checked in the conditioned media from HMVEC-D cells treated with IL-1β in the presence or absence of Actinomycin-D and Cycloheximide by ELISA.

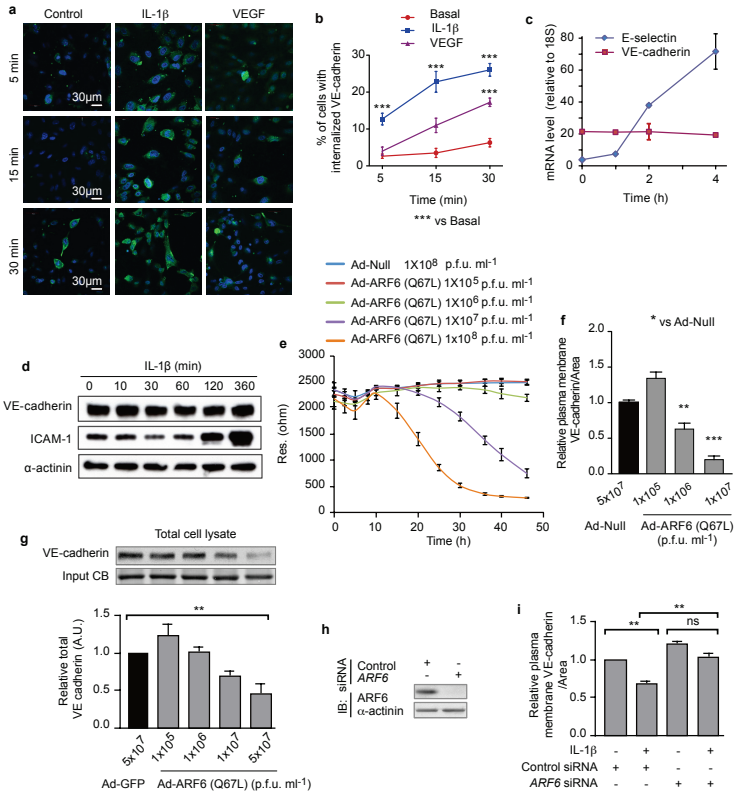

Supplementary Figure 4. ARF6 constitutive activation enhances vascular permeability.
(a) Immunofluorescence of internalized VE-cadherin (green) in IL-1β and VEGF stimulated HMVEC-D cells after 5, 15, and 30 minutes. **(b)** Quantification of VE-cadherin internalization in IL-1β and VEGF stimulated HMVEC-D cells after 5, 15, and 30 minutes. Induction of VE-cadherin internalization by IL-1 β is more rapid than that induced by VEGF. **(c)** VE-cadherin and E-selectin mRNA levels in IL-1β-stimulated HMVEC-D cells. **(d)** Lysates from IL-1β-stimulated HMVEC-D were immunoblotted with antibodies against VE-Cadherin and ICAM-1 at various time points. **(e)** HMVEC-D cells infected with Ad-Null or Ad-ARF6 (Q67L) adenovirus were assessed for transendothelial resistance by ECIS. **(f)** Quantification of Figure 2e. **(g)** Immunoblotting for VE-cadherin of cell lysates or from ARF6 (Q67L) adenoviral-vector infected HMVEC-D. **(h)** Lysates from HMVEC-D cells transfected with *ARF6* or control siRNA were immunoblotted for ARF6. **(i)** Quantification of Figure 1j. For all experiments, N ≥ 3, and error bars represent SEM. * p<0.05, ** p<0.01, *** p<0.001, **** p<0.0001.

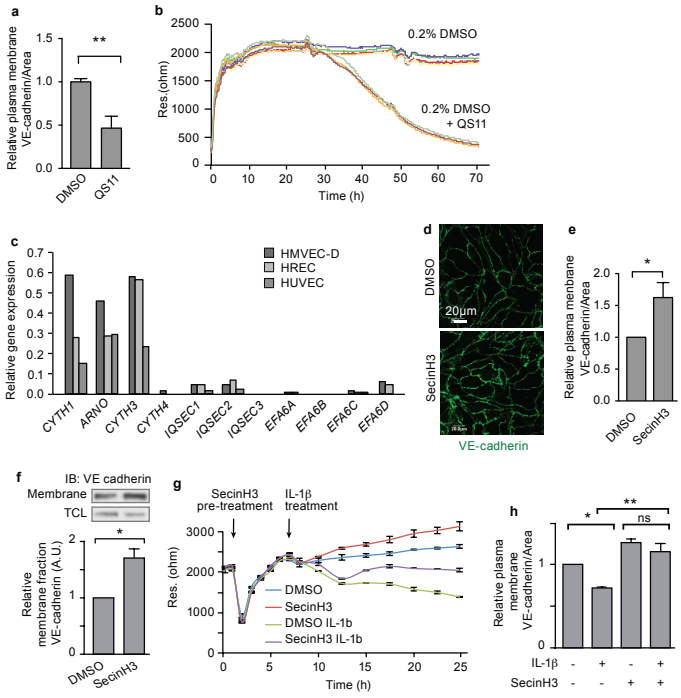

Supplementary Figure 5. Inhibition of ARF-GAPS or ARF-GEFs with small molecules decreases or increases VE-cadherin cell-surface localization respectively.
(a) Quantification of plasma membrane VE-cadherin as shown in Figure 3c. **(b)** Transendothelial resistance was measured by ECIS in HMVEC-D cells treated with DMSO or QS11. **(c)** HMVEC-D, Human retinal endothelial cells (HREC), and Human umbilical vein endothelial cells (HUVEC) were analyzed by quantitative RT-PCR for ARF-GEF, CYTH, IQSEC and EFA6 family gene expression. **(d)** HMVEC-D cells stimulated with DMSO or SecinH3 were subjected to immunofluorescence for VE-cadherin (green). **(e)** Quantification of (d). **(f)** VE-cadherin membrane fraction after treatment with SecinH3 or DMSO control. **(g)** Transendothelial resistance was measured in HMVEC-D cells stimulated with IL-1β in the presence of DMSO or SecinH3 by ECIS. **(h)** Quantification of Figure 2g. For all experiments, N ≥ 3, and error bars represent SEM. * p<0.05, ** p<0.01, *** p<0.001, **** p<0.0001.

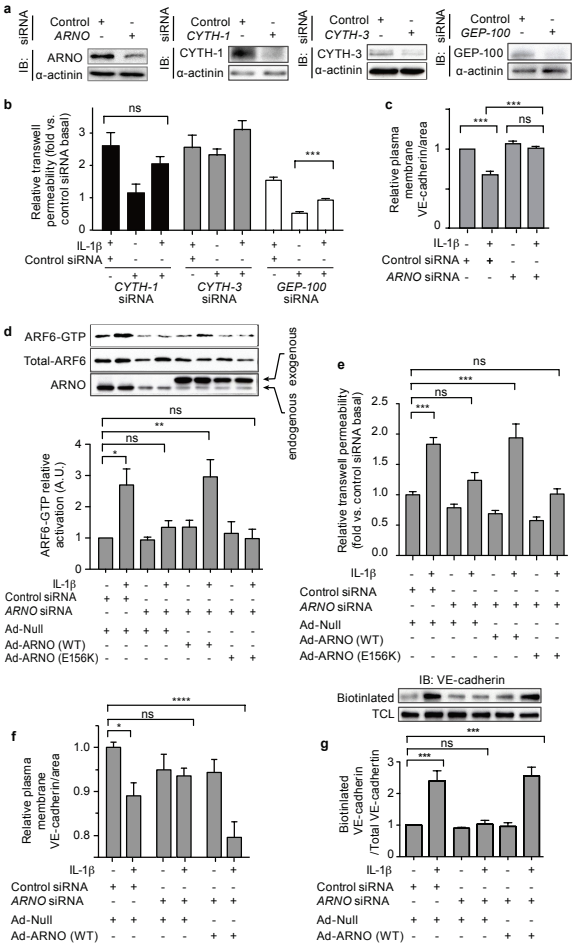

Supplementary Figure 6. The ARF-GEF ARNO/Cytohesin-2 is critical for modulating IL-1β-induced VE-cadherin localization.

(a) Lysates from HMVEC-D cells transfected with *Cytohesin-1, ARNO, Cytohesin-3, GEP-100* or control siRNA were immunoblotted for Cytohesin-1, ARNO, Cytohesin-3, or GEP-100. **(b)** Transwell permeability of *Cytohesin-1, Cytohesin-3, GEP-100* or control siRNA treated HMVEC-D stimulated with IL-1β for 2 hours. We show that loss of cytohesin-1 or cyothesin-3 have no effect in IL-1β induced permeability. Additionally, while loss of GEP-100 decreases baseline permeability, there is no effect on the fold increase in IL-1β induced permeability, suggesting that GEP-100 is regulating permeability independent of an IL-1β pathway. **(c)** Quantification of Figure 2k. **(d)** HMVEC-D treated with *ARNO* or control siRNA were stimulated with IL-1β in the presence or absence of Ad-ARNO-MYC or Ad-Null then assayed by GTP-ARF6 pulldown and immunoblotted with ARF6 antibodies. **(e)** HMVEC-D treated with *ARNO* or control siRNA were infected with Ad-Null or *ARNO* siRNA resistant Ad-ARNO-MYC, then stimulated with IL-1β and assayed by transwell permeability assay. **(f)** Quantification of cell-surface VE-cadherin in HMVEC-D treated with *ARNO* or control siRNA and infected with Ad-Null or *ARNO* siRNA resistant Ad-ARNO-MYC, then stimulated with IL-1β as in (e). **(g)** Immunoblot for biotin-labeled internalized VE-cadherin after IL-1β stimulation in conditions described in (e) and (f). For all experiments, N ≥ 3, and error bars represent SEM. * p<0.05, ** p<0.01, *** p<0.001, **** p<0.0001.

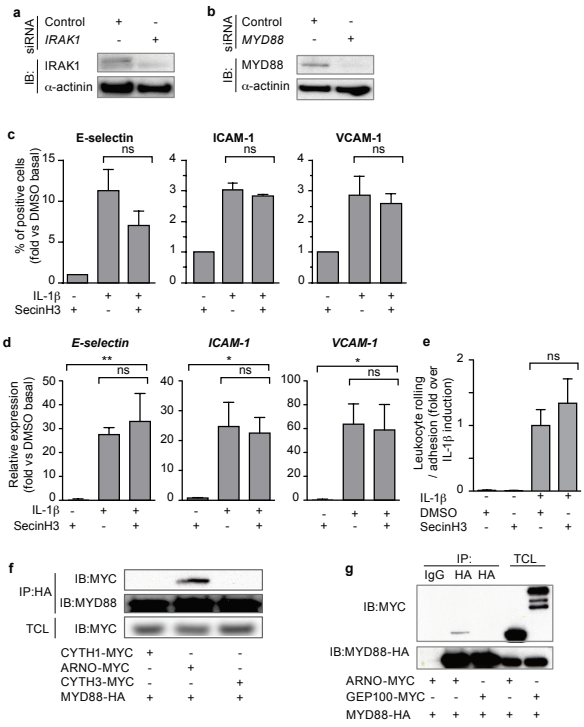

Supplementary Figure 7. The IL-1β-induced permeability pathway diverges from the canonical NF-κB pathway at MYD88.
(a) Lysates from HMVEC-D cells transfected with *IRAK1* or control siRNA were immunoblotted for IRAK1. **(b)** Lysates from HMVEC-D cells transfected with *MYD88* or control siRNA were immunoblotted for MYD88. **(c)** Fluorescence-activated cell sorting for E-selectin, ICAM-1 and VCAM-1 cell surface localization of HMVEC-D stimulated with IL-1β in the presence of DMSO or SecinH3. **(d)** Quantitative RT-PCR for *E-selectin, ICAM-1* and *VCAM-1* of HMVEC-D stimulated with IL-1β in the presence of DMSO or SecinH3. **(e)** Quantification of human polymorphonuclear leukocyte rolling and adherence to a HMVEC-D monolayer under shear stress conditions. **(f)**, **(g)** Lysates from HEK 293T cells expressing MYD88-HA and the indicated ARF-GEF-MYC constructs were immunoprecipitated with anti-HA antibodies and immunoblotted with anti-MYC antibodies. For all experiments, N ≥ 3, and error bars represent SEM. * p<0.05, ** p<0.01, *** p<0.001, **** p<0.0001.

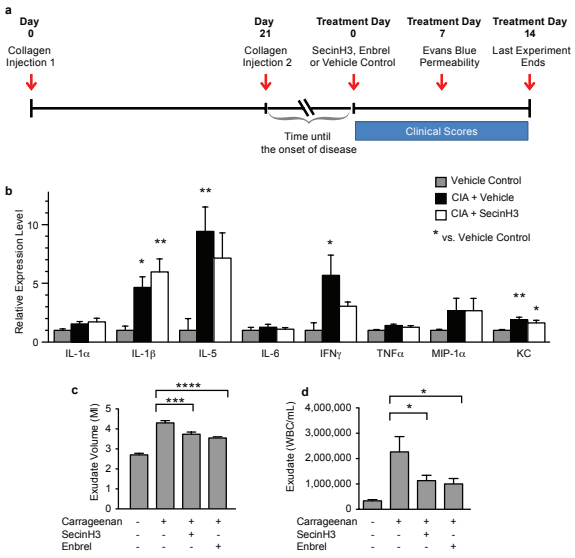

Supplementary Figure 8. The effects of SecinH3 treatment in the collagen-induced arthritis and air-pouch models.
(a) Timeline of the collagen-induced arthritis assay. Arthritis was induced by two collagen injections 21 days apart. Mice were segregated into pools and treatment with SecinH3, Enbrel, or Vehicle Control was initiated after the onset of disease. Evans Blue experiments were performed seven days after treatment initiation. Clinical scores were recorded daily from the day of treatment initiation until the experiment ended 14 days later. **(b)** Measurement of cytokine levels within arthritic joints 24 hours post treatment initiation. In an air-pouch model of acute inflammation, exudate volume **(c)**, as well as the white blood cell concentration **(d)** in the exudates was measured in the vehicle, SecinH3, or Enbrel-treated mouse six hours after inflammatory stimulus. Error bars represent SEM for 6-8 mice per group. * $p<0.05$, ** $p<0.01$, *** $p<0.001$, **** $p<0.0001$.

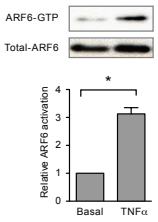

Supplementary Figure 9. TNFα activates ARF6 in endothelial cells.
HMVEC-D cells stimulated with TNFα were assayed by ARF6-GTP pull down assay and then immunoblotted with anti-ARF6 antibodies. Experiments, N=3, and error bars represent SEM. * $p<0.05$.

METHODS

Reagents

Human dermal microvascular endothelial cells (HMVEC-D) were purchased at passage 0 from Lonza and used at passages 2-6. SecinH3, ERK1/2 signal pathway inhibitor (U0126), P38 signal pathway inhibitor (SB203580), JNK signal pathway inhibitor (JNK Inhibitor II), and NF-κB signal pathway inhibitor (SC-514) were from Calbiochem. QS11 was from Sigma. Rabbit anti-VE-cadherin antibody, rabbit anti-MYD88 antibody (#3699 for western blot, #4283 for immunoprecipitation), rabbit anti-IRAK1 antibody, rabbit anti-p-ERK1/2, rabbit anti-p-P38, rabbit anti-p-JNK antibody, rabbit anti-ERK1/2, rabbit anti-P38 antibody, rabbit anti-JNK antibody and rabbit anti-NF-κB P65 antibody were from Cell Signaling. Mouse anti-ARF6 antibody was from Millipore. Mouse anti-ARNO antibody was from Abnova. *ARF6* siRNA, *ARNO* siRNA, *MYD88* siRNA and *IRAK1* siRNA were from Qiagen.

Transfection and siRNAs

siRNAs were diluted in 12.5% HiPerFect Transfection Reagent (Qiagen) in Optimem (Invitrogen) and incubated 10-20 minutes at room temperature. As siRNAs were sitting, passage 3-4 HMVEC-D cells were passaged and resuspended in EGM2-MV (Endothelial Cell Basal medium-2 supplied with EGM®-2 MV SingleQuots®, Lonza) and combined with siRNAs such that the final concentration of siRNA was 30nM (all targets). The cells were plated, allowed to grow overnight and then the growth media was replaced. Three days after the initial transfection, the cells were transfected a second time using the same HiPerFect/siRNA concentrations as above.

The following is a table of all siRNAs used, their catalogue numbers, sequence, the location within the gene the siRNA targets, and average knockdown observed by western blot.

Gene	Catalogue Number	Target sequence (5'-3')	Region	Mean knockdown
ARF6	SI02757286	CAACGTGGAGACGGTGACTTA	exon	77%
ARNO	SI00061299	CACGCTGTTGGTAATCTTATT	3' UTR	63%
Cytohesin-1	SI04217185	CGGGACAGAGGTTCCGGATAA	3' UTR	93%
Cytohesin-3	SI00061257	CAGCATGTTGTGCTCGGACAA	3' UTR	99%
MYD88	SI00300909	AACTGGAACAGACAAACTATC	exon	87%
IRAK1	SI00605262	CCGGGCAATTCAGTTTCTACA	exon	83%

Protein expression constructs

The coding sequence of full-length *MYD88* (BC023589), *ARNO* (BC038713), *CYTH-1* (BC038385), *CYTH-3* (BC028717) and *GEP100* (BC010267) were amplified by PCR from IMAGE cDNA clones and ligated into a **pcDNA3.1** vector after enzyme digestion. The ARNO, CYTH-1, CYTH-3 and GEP100 constructs contained both MYC and HIS epitopes, while the MYD88 construct contained an HA epitope.

Subcellular fractionation

Subcellular fractionation was performed as previously described[9]. Briefly, HMVEC-D cells were infected with adenovirus for 48 hours, stimulated with QS11 for 3 hours, or stimulated with SecinH3 for 2 hours. Alternatively, cells were transfected with siRNA as described above. The monolayer was washed two times with ice-cold phosphate-buffered saline (PBS) containing Ca^{2+} and Mg^{2+}, and then washed a third time with HLB buffer [Tris-HCl 10mM at pH 7.4, KCl 5mM,

protease inhibitors (Roche) and phosphatase inhibitors (Sigma), and dithiothreitol 1mM]. After the third wash, cells were homogenized in a Dounce homogenizer using 20 strokes. The homogenate was then centrifuged at 400g for 10 minutes at 4˚C. The supernatant was subjected to centrifugation again at 16,000g for 30 minutes at 4˚C. The pellet was washed with HLB buffer and resuspended in radioimmunoprecipitation assay (RIPA) buffer for 30 minutes at 4˚C. The resuspended pellet was centrifuged at 16,000g for 15 minutes at 4˚C, and the supernatant was saved as a soluble membrane fraction. To obtain the total cell lysate, an aliquot of cellular material was set aside before Dounce homogenization. RIPA buffer was added to this aliquot and then the mixture was centrifuged at 13,000g for 10 minutes at 4˚C. The resulting supernatant was saved for use as total cell lysate. Densitometry was performed on at least three independent experiments and data are presented as mean ± SEM.

ARNO Rescue Experiment

Cells (1.0×10^6 in a 10 cm dish) were first transfected with *ARNO* siRNA (SI00061299, Qiagen) at 30nM and changed to fresh media 24 hours after the transfection. The siRNA was directed against sequences in the 3' UTR of the endogenous *ARNO* mRNA. 48 hours after the media change, cells were harvested and underwent a second transfection with the same siRNA at the same dose. Cells were then infected with either an Ad-ARNO (WT) or Ad-ARNO (E156K) virus (5×10^7 p.f.u.ml^{-1}) 36 hours after the second siRNA transfection and incubated for 36 hours[2]. The adenoviral vectors expressing human ARNO (or mutant ARNO) fused to a MYC-epitope tag did not contain a 3'UTR *ARNO* sequence, and was thus predicted to be resistant to the siRNA.

ARF6-GTP pull down assay: ARF6-GTP pull-down assays were performed as described[21]. Briefly, HMVEC-D cells were pre-treated with SecinH3 for 3 hours followed by treatment with

10ng/mL IL-1β. Alternatively, cells were transfected with siRNA as described above. Cells were treated with IL-1β 72 hours after the second siRNA transfection for 5 minutes. After treatment, media was aspirated and cells were rinsed with chilled Ultrasaline. Dishes were frozen on dry ice. Following thawing, ARF6 pulldown lysis buffer [Tris-HCl 50mM, NaCl 100mM, $MgCl_2$1mM, NP-40 1%, glycerol 10%, protease inhibitors (Roche) and phosphatase inhibitors (Sigma)] were added to cells. Lysates were centrifuged and supernatants were added to GGA3-conjugated beads (Cell Biolabs, sta-40706), and agitated at 4°C for 60 minutes. Beads were washed in ARF6 pulldown lysis buffer and resuspended in 2X Laemmli prior to loading on 15% SDS-PAGE gels. A fraction of the cell lysate was withheld for use as a measure of total ARF6 in each sample. Data are presented as mean ± SEM of at least three independent experiments.

Quantitative PCR

Total RNA was extracted from cells using the RNeasy plus mini kit (Qiagen) according to manufacturer's instructions. RNA was converted to cDNA using RETROscript® kit (Ambion). Quantitative RT-PCR was performed using TaqMan probes (*CYTH1*, Hs00245092; *ARNO*, Hs00244669; *CYTH3*, Hs00188456; *CYTH4*, Hs00203581; *IQSEC1*, Hs00208333; *IQSEC2*, Hs00390333; *IQSEC3*, Hs01006522; *EFA6A*, Hs00160539; *EFA6B*, Hs00260268; *EFA6C*, Hs00209633; *EFA6D*,Hs00202892; *VEGFA*, Hs00900055; *ICAM1*, Hs00164932; *VCAM1*, Hs01003372; *IL-6*, Hs9999032; *TNFα*, Hs01113624_g1; *Cox2*, Hs00153133; *VE-cadherin*, Hs00901463; *E-selectin*, Hs00174057_m1) and the ABI Prism 7900 HT Real-Time PCR System (Applied Biosystems). Quantification was performed using a human brain cDNA standard curve and normalized to 18S rRNA. Data are presented as mean ± SEM of four duplicates from at least two independent experiments.

Immunofluorescence

10,000 HMVEC-D cells were seeded onto 8 well chamber slides coated with human fibronectin. Cells were pre-treated with small molecule inhibitors of NF-κB or MAPK for 30 minutes or SecinH3 for 3 hours followed by treatment with 10 ng/ml IL-1β for 2 hours. Alternatively, cells were infected with 1×10^{5}-1×10^{8} p.f.u.ml^{-1} of the indicated adenovirus for 48 hours. For siRNA knockdown experiments, cells were harvested 72 hours after the first siRNA transfection, re-transfected with the same siRNA a second time and seeded onto chamber slides. 72 hours after the second siRNA transfection, cells were treated with IL-1β for 2 hours. Cells were fixed, permeabilized, blocked with normal donkey serum and stained for VE-cadherin or NF-κB p65. The only exception to this protocol was for Supplementary Fig. 6f, where permeabilization was not performed in order to increase the signal of cell-surface VE-cadherin. Images are maximum-Z-projections of confocal images acquired at 0.3 μm z-section intervals. Image acquisition settings were identical for all images. Images are representative of at least 3 independent experiments. Quantification was performed using a custom Image-J macro that imported images, applied a threshold to exclude all but intensely-stained areas, and returned this area as an output. Identical threshold and size restriction values were used to analyze all images. Data are presented as mean ± SEM of at least three independent experiments.

Immunoprecipitation

Immunopreciptation assays were performed as described[9]. Briefly, HMVEC-D cells were treated with 10 ng/ml IL-1β for 1 and 5 minutes. For Figure 3e, HMVEC-D cells were infected with 1×10^{7} p.f.u.ml^{-1} Ad Null or Ad-ARNO-MYC 48 hours before IL-1β treatment. Cells were then washed with ice-cold PBS and lysed with ice-cold lysis buffer (Tris-HCl 50 mM, NaCl

250mM, NP-40 1%, and glycerol 10% with protease inhibitors and phosphatase inhibitors). Cell lysates were centrifuged for 15 minutes at 13,000g and the supernatants saved. A BCA assay (Pierce) was used to determine protein concentrations. Lysates were incubated with 8 mg of the indicated antibody and protein A/G–Sepharose (Santa Cruz Biotechnology) for 1 hour at 4°C. Beads were then washed 5 times in lysis buffer. The immunoprecipitates were assayed by western blot analysis using Peroxidase-conjugated AffiniPure Light Chain Specific secondary antibody for signal detection. Data represents at least 3 independent experiments.

Biotinylation Assay

HMVEC-D cells were transfected with *ARNO* siRNA or control siRNA and then infected with Ad null or Ad-ARNO (as described), and grown to 100% confluence on 100-mm dishes. Cells were washed with ice-cold PBS three times and labeled with EZ-link Sulfo-NHS-SS-Biotin (Thermo) at 0.5mg/ml in PBS for 30 minutes on ice. Excess Biotin was removed by washing with glycine in PBS two times on ice. The cells were then incubated with 10 ng/ml IL-1β and 0.6 mM Primaquine (MP Biomedicals) at 37°C for 30 minutes; they were then exposed to GSH buffer (Glutathione 50mM, NaOH 75mM, NaCl 75mM, EDTA 1mM, BSA 0.1%, PH 9.0) on ice for 20 minutes to remove surface biotin. GSH was then quenched by washing with 5 mg/ml iodoacetamide in PBS. After an additional wash with ice-cold PBS, cells were lysed in NP-40 buffer (Tris-HCl 50 mM, NaCl 150 mM, MgCl2 1mM, NP-40 1%, Glycerol 10%) with a protease inhibitor cocktail on ice. Cell lysates were centrifuged at 14,000 rpm for 15 minutes and supernatant was incubated with High Capacity Streptavitin Agarose Resin (Thermo) for 60 minutes at 4°C. Beads were washed with NP-40 lysis buffer three times. Bound proteins were released in 2×Laemmli buffer with 5% β-mercaptoethanol at 95°C and internalized VE-cadherin analyzed by immunoblotting with VE-cadherin antibody.

Transendothelial resistance

Transendothelial resistance was measured by Electric Cell-substrate Impedance Sensing (ECIS). An 8W10E+ electrode culture array (Applied Biophysics) was coated with 10 µg/mL human fibronectin. 5 x 10^4 HMVEC-D per well were seeded in complete media onto the electrode culture array and monitored until a stable monolayer formed. A stable monolayer was indicated by a capacitance <10 nF at 6.4 x 10^4 Hz and a stable resistance over several hours at 4 x 10^3 Hz. Cells were pre-treated with SecinH3/Avastin for 3 hours or MAPK/NF-κB inhibitors or Indomethacin or PGE_2 for 30 minutes followed by treatment with 10 ng/ml IL-1β (unless otherwise indicated). Alternatively, cells were infected with Ad-GFP or Ad-ARF6 (Q67L) adenoviruses. Resistance across the monolayer using alternating current at a frequency of 4 x 10^3 Hz was measured by 40 electrodes per well (1000-2000 cells) using the ECIS-Zθ system (Applied Biophysics) and reported in Ohms or normalized to control treatment or initial resistance. Conditioned media was collected from cells undergoing ECIS (Supplemental Figure 2e) at 16 hours after treatment with IL-1β in the presence of DMSO or inhibitors. PGE_2 concentration was calculated using the PGE_2 Express EIA kit from Cayman Chemical (500141) according to manufacturer's instructions. Data are representative of at least 3 independent experiments or represented as mean ± SEM.

Transwell permeability

HMVEC-D cells were seeded on 1.0 µm Costar transwell inserts coated with fibronectin. Cells were grown to confluency and treated with SecinH3 for 3 hours or MAPK/NF-κB/transcription/translation inhibitors for 30 minutes followed by treatment with 10ng/ml IL-1β. Alternatively, cells were infected with Ad-GFP or Ad-ARF6 (Q67L) adenovirus for 48 hours.

siRNA knockdown was performed as described and cells were treated with IL-1β 72 hours after the second siRNA transfection. Two hours later, horseradish peroxidase (HRP) was added to the top chamber at a final concentration of 100μg/ml. Medium was removed after 60 minutes from the lower chamber. For time-course transwell assays and transcription/translation inhibitor experiments (Figure 1a, d), HRP was added to the insert at the same time as IL-1β. Transwell inserts were moved to fresh wells after each timepoint, and the concentration of HRP in the bottom chamber was measured for monolayer permeability. HRP was assessed using media samples obtained from the lower chamber incubated with 0.5 mM of guaiacol and 0.6 mM H_2O_2. Spectrophotometric analysis of absorbance at 490 nm provided a quantitative evaluation of the amount of HRP that crossed the membrane. Data are presented as mean ± SEM of at least three independent experiments performed in quadruplicate.

Fluorescence-Activated Cell Sorting (FACS)

FACS was performed as decribed[31]. HMVEC-D were pre-treated with SecinH3 for 3 hours and then stimulated with 10 ng/ml IL-1β for 4 hours. Analysis of the cell surface localization of adhesion molecules was performed with one step immunofluorescence staining using anti-hE-selectin-FITC, anti-hICAM1-FITC and anti-hVCAM1-PE antibody (BD). Data are presented as mean ± SEM of at least three independent experiments.

Leukocyte Rolling and Adherence assay

3 x 10^4 HMVEC-D were seeded into each well of a fibronectin-coated parallel plate flow chamber (U-plate 0.4 VI Fibronectin, Ibidi GMBH). Media was changed daily using gentle aspiration until the cells had grown to confluence (approximately 3-5 days). Human polymorphonuclear leukocytes (PMNs) were isolated from whole blood according to previously

described protocols[32,33]. Briefly, human peripheral venous blood (500 mL) from healthy, medication-free, fasting adult subjects was drawn into acid-citrate-dextrose (1.4 mL ACD/8.6 mL blood) through standard venipuncture technique and used immediately upon collection. The University of Utah Institutional Review Board approved this study and all subjects provided informed consent. Blood was centrifuged at 150 x g for 20 minutes at 20°C to separate platelet-rich plasma (PRP) from red and white blood cells (RBC/WBC). The PRP was removed and the remaining RBC/WBC mixture was resuspended in 0.9% sterile saline back to the original volume. A volume equaled to half the original blood volume of 6% Dextran 70 (Sigma-Aldrich, St. Louis, MO) was then added to the RBC/WBC mixture and left for one hour. The leukocyte-rich supernatant was removed and centrifuged at 400 x g for five minutes a 4°C. The supernatant was then removed and the pellet resuspended (in 0.2% NaCl followed by an equal part of 1.6% NaCl), and the cells were centrifuged at 400 x g for five minutes at 4°C. After centrifugation, the cells were resuspended in Hank's Balance Salt Solution (Sigma-Aldrich, St. Louis, MO) with 1% human serum albumin (HBSS/A) (University of Utah Hospital, Salt Lake City, UT) and layered over an equal volume of Ficoll-Paque Plus (GE Healthcare Biosciences, Piscataway, NJ). The layered cells were then centrifuged for 30 minutes at 400 x g at 4°C. After 30 minutes, the mononuclear leukocyte layer was removed, followed by the RBC layer, HBSS/A layer, and Ficoll-Paque layer. The remaining pellet containing greater than 95% PMNs was washed with HBSS/A and resuspended to 1 x 10^6 ml^{-1} in warmed ultrasaline (Lonza). Endothelial cells in parallel-plate flow chambers were pretreated with IL-1β (10 ng/mL) and/or SecinH3 for 3 hours. A syringe pump (Harvard Apparatus) was used to flow the PMN solution through the parallel plate flow chambers at 1 dynes x cm^{-1} (a typical venous shear stress). Differential Interference contrast microscopy (DIC) images were taken once per second using an Olympus inverted

microscope, and the total number of PMNs rolling and adhered in a 5 minute period were quantified using MetaMorph (Olympus) software. The data is presented as fold over IL-1β induced leukocyte rolling ± SEM and represents three independent experiments, each consisting of at least 3 replicates for each condition.

Internalization assay

VE-cadherin internalization assay was performed as previously described[9]. Briefly, HUVEC were transfected with siRNA as described above and seeded onto 8-well chambered coverglass at 5 x 10^4 cells/coverglass. After 72 hours, the culture was chilled at 4˚C for 30 minutes, surface-labeled for 60 minutes on ice with 1 ug/mL dialyzed anti-VE Cadherin antibody (clone BV6, Millipore) in ice-cold labeling buffer (3% BSA in MCDB131 medium, Invitrogen). At the end of 60 minutes, the labeling buffer was removed and the cells were treated with 0.6 mM Primaquine plus vehicle or 10 ng/mL IL-1β, DMSO vehicle or 30 μM SecinH3 or 50 μM SC-514 for 15 minutes at 37˚C and 5% CO2. Monolayers were washed 3 times over 10 minutes with ice-cold HBSS (HBSS - Hank's Balanced Salt Solution, Invitrogen) + 50mM Glycine + 3% BSA, pH 2.7 to remove surface VE-cadherin. One well for each condition was washed in a neutral pH solution to retain surface VE-cadherin staining. Subsequently, monolayers were fixed immediately in 3% paraformaldehyde for 10 minutes. The VE-cadherin antibody was detected using an Alexa-Fluor 488 conjugated anti-Mouse IgG antibody and traditional immunofluorescence methods. To image the monolayers, five images per well were randomly selected using the DAPI channel at 600x. Z-series images were taken using a confocal Olympus FV1000IX81 microscope. Each treatment was done in triplicate. The assay score represents the average percentage of total cells in each image/well/treatment containing internalized VE-Cadherin.

Collagen-induced arthritis

Collagen-induced arthritis (CIA) studies were conducted by Washington Biotechnology using their standard procedures and DBA/1J mice as previously published[34-38]. All protocols were approved by their IACUC (Institutional Animal Care and Use Committee) prior to initiation of the study. Six to seven week old male DBA/1 mice were used (Jackson Laboratories) with 5-20 animals per group. Bovine type-II collagen (Chondrex) was dissolved in 0.01 M acetic acid, and an emulsion with 50 µl of Complete Freund's Adjuvant was injected at the base of the tail at Day 0. 21 days following the first injection, a booster injection consisting of a 50 µL emulsion of collagen in Incomplete Freund's Adjuvant was injected at the base of the tail. Arthritic index (AI) was scored for each limb of an animal as follows: 0 = no visible effects of arthritis, 1 = edema and erythema of one digit or joint, 2 = edema and erythema of two joints, 3 = edema and erythema of more than 2 joints, 4 = severe arthritis of the entire paw and digits accompanied by deformity of the limb. The score for each limb was summed, with 16 as the highest possible AI score for each animal. Treatments were either vehicle (0.5% DMSO/saline IP BID), SecinH3 (0.1 mg/kg IP BID), or the positive control, Enbrel® (10 mg/kg SC OD). The experiment was repeated multiple times with different endpoints; detailed descriptions of the exact timing for each experiment follow. In all cases, treatment was initiated after mild arthritis was established (therapeutic treatment).

EVAN's BLUE DYE EXTRAVASATION: Treatment was initiated when the average arthritic index for each group was between 3.4 - 3.55 and all mice in each group demonstrated a positive arthritic index. Due to the variation in when each group reached an average arthritic index of 3.4 – 3.55, treatment initiation day varied from study day 28 (seven days after the second collagen injection) to study day 30 (nine days after the second collagen injection). The treatments lasted

for seven days until the mice were sacrificed for the Evan's Blue Dye Assay (described in detail in subsequent methods).

ARTHRITIS PROGRESSION: Treatment was initiated when the average arthritic index for each group was 3.1 and all mice in each group demonstrated a positive arthritic index. Due to the variation in when each group reached an average arthritic index of 3.1, treatment initiation day varied from study day 28 (seven days after the second collagen injection) to study day 29 (eight days after the second collagen injection). The treatments lasted for 13 days in all groups with arthritic index recorded regularly throughout.

HISTOPATHOLOGIC PATTERNS: Treatment was initiated when the average arthritic index for each group was between 3.1-3.2 and all mice in each group demonstrated a positive arthritic index. Due to the variation in when each group reached an average arthritic index of 3.1 - 3.2, treatment initiation day varied from study day 29 (eight days after the second collagen injection) to study day 33 (12 days after the second collagen injection). The treatments lasted for 14 days in all groups before joints were harvested for histology. Limbs were preserved in 10% neutral buffered formalin for histology. Limbs were decalcified in formic acid for 2-3 days, paraffin embedded, and 8 μm sections stained with toluidine blue. Arthritis severity was evaluated for inflammation, pannus, cartilage damage, and bone damage.

CYTOKINE EVALUATION: Treatment was initiated when the average arthritic index for each group was 3.4 and all mice in each group demonstrated a positive arthritic index. All groups reached an average arthritic index of 3.4 on day 34 (13 days after the second collagen injection), and treatment was initiated. The treatments lasted for 1 day, at which time plasma and ankle joints were collected for cytokine analysis (described in detail in subsequent methods).

All selection and later scoring were blinded to treatment. Data are represented as mean ± SEM.

CIA - Cytokine or chemokine array

CIA was induced as described. 24 hours after treatment of SecinH3, joints of mice were collected and pulverized using a mortar and pestle filled with liquid nitrogen. Tissue was transferred to 15 ml tubes, resuspended in 1 ml PBS and homogenized using a Polytron tissue homogenizer (*PRO* Scientific Inc. USA) for 20 s. Mouse joint homogenates were centrifuged for 10 minutes at 500 g at 4°C. Supernatants were transferred to 1.5 ml Eppendorf tubes, centrifuged at 15,000 g for 5 minutes and collected for cytokine analysis by Quansys Biosciences. Data are presented as mean ± SEM for 6 mice per condition.

CIA – Evans Blue permeability

CIA was induced as described. Seven days after randomization and treatment initiation, mice were given an IV injection of 5 ml/kg of 1% Evans Blue dye. One hour later, mice were bled and plasma collected. Mice were perfused, the hind limbs degloved, and ankle joints homogenized in 0.5 ml saline. 1.5 ml formamide was added and Evans Blue dye eluted overnight at 60°C. Supernatant and plasma samples were read spectrophotometrically and expressed as OD620-OD740 joints divided by OD620-OD740 plasma. Values were normalized to non-CIA-induced mice and expressed as fold increase over control. N=14 per group and data are represented as mean ± SEM.

Air-Pouch Model

The Carrageenan-induced Air Pouch Model was performed by Washington Biotechnology as previously described[39-41]. All protocols were approved by their IACUC (Institutional Animal

Care and Use Committee) prior to initiation of the study. Six to seven week old male Swiss-Webster mice were used (Harlan) with 6-8 animals per group. On day 0, the nape of the neck was shaved and six mL of sterile air was injected subcutaneously. On day 3, three mL of sterile air was injected subcutaneously. On days 4 and 5, mice that were to be induced at a later time were injected with either 0.1 mg/kg SecinH3 IP BID, vehicle IP BID, or 10 mg/kg Enbrel® SQ QD. On day 6 an additional injection was administered one hour prior to carrageenan injection. One mL of 3% carrageenan (FLUKA) previously prepared in de-ionized water with heat, or 1mL of saline for the sham group, was then injected into the air pouch. Four hours after carrageenan injection, the mice were anesthetized and 3mL of 10 U/mL heparinized saline was injected into the air pouch. The air pouch was gently massaged, the contents immediately removed, and the exudate volumes recorded. An aliquot of the exudate was transferred to heparin-treated microtainer tubes for differential white blood cell counting. Samples with bloody exudates were discarded from white blood cell counting.

Statistical analysis

For the majority of data, one-way ANOVA (analysis of variance) with Tukey's post-hoc test was used to assess statistical significance. A Student's t-test was used when the experiment was only composed of two groups. Two-way ANOVA with Bonferroni post-hoc test was used to assess statistical significance for data shown in Figure 4b. A *P*-value of less than 0.05 was considered statistically significant. Unless otherwise noted, P-values of less than 0.05 are denoted with a single symbol (ie. *); P-values less than 0.01 are denoted with two symbols (ie **); P-values less than 0.001 are denoted with three symbols (ie ***); P-values less than 0.0001 are denoted with four symbols (ie ****), etc.

Methods References

31 Jones, C.A. *et al.* Robo4 stabilizes the vascular network by inhibiting pathologic angiogenesis and endothelial hyperpermeability. *Nature Medicine* **14**, 448-453 (2008).

32 Zimmerman, G.A., McIntyre, T.M., & Prescott, S.M. Thrombin stimulates the adherence of neutrophils to human endothelial cells in vitro. *J. Clin Invest* **76**, 2235-2246, (1985)

33 Yost, C.C. *et al*. Activated polymorphonuclear leukocytes rapidly synthesize terinoic acid receptor-alpha: a mechanism for translтional control of transcriptional events. *J Exp Med* **200**, 671-680, (2004).

34 Zimmerman, D.H. *et al*. Cel-2000: A therapeutic vaccine for rheumatoid arthritis arrests disease development and alters serum cytokine/chemokine patterns in the bovine collagen type II induced arthritis in the DBA mouse model. *Int immunopharmacol* **10**, 412-421, (2010).

35 Zalevsky, J. *et al.* Dominant-negative inhibitors of soluble TNF attenuate experimental arthritis without suppressing innate immunity to infection. *J Immunol* **179**, 1872-1883, (2007).

36 Konda, V. R., Desai, A., Darland, G., Bland, J. S. & Tripp, M. L. META060 inhibits osteoclastogenesis and matrix metalloproteinases in vitro and reduces bone and cartilage degradation in a mouse model of rheumatoid arthritis. *Arthritis Rheum* **62**, 1683-1692, (2010).

37 Miner, J. N. *et al.* Antiinflammatory glucocorticoid receptor ligand with reduced side effects exhibits an altered protein-protein interaction profile. *Proceedings of the National Academy of Sciences of the United States of America* **104**, 19244-19249, (2007).

38 Montalban, A. G. *et al.* KR-003048, a potent, orally active inhibitor of p38 mitogen-activated protein kinase. *Eur J Pharmacol* **632**, 93-102, (2010).

39 Colville-Nash, P. & Lawrence, T. Air-pouch models of inflammation and modifications for the study of granuloma-mediated cartilage degradation. *Methods Mol Biol* **225**, 181-189, (2003).

40 Cronstein, B. N., Montesinos, M. C. & Weissmann, G. Salicylates and sulfasalazine, but not glucocorticoids, inhibit leukocyte accumulation by an adenosine-dependent mechanism that is independent of inhibition of prostaglandin synthesis and p105 of NFkappaB. *Proceedings of the National Academy of Sciences of the United States of America* **96**, 6377-6381 (1999).

41 Edwards, J. C., Sedgwick, A. D. & Willoughby, D. A. The formation of a structure with the features of synovial lining by subcutaneous injection of air: an in vivo tissue culture system. *J Pathol* **134**, 147-156, (1981).

CHAPTER 3

ARF6 INHIBITION STABILIZES THE VASCULATURE AND ENHANCES SURVIVAL DURING ENDOTOXIC SHOCK

The following chapter was reprinted with permission from the American Association of Immunology. My co-authors were Weiquan Zhu, Christopher C. Gibson, Jay Bowman-Kirigin, Lise Sorensen, Jing Ling, Huiming Sun, Sutip Navankasattusas, and Dean Y. Li. In this manuscript published in the Journal of Immunology, May 16, 2014, doi:10.4049/jimmunol.1400309, we showed that a MYD88-ARNO-ARF6 axis controls permeability induced by bacterial lipopolysaccharides and we characterized an inhibitor of ARF6 that reduces vascular permeability in both *in vitro* and *in vivo* settings as well as enhances survival in lethal endotoxemia models. Also in this chapter is an appendix including a set of experiments that describes the antimicrobial nature of an inhibitor of ARF6, MyrARF6 2-13.

Published May 16, 2014, doi:10.4049/jimmunol.1400309

ARF6 Inhibition Stabilizes the Vasculature and Enhances Survival during Endotoxic Shock

Chadwick T. Davis,[*,†,‡] Weiquan Zhu,[†,‡] Christopher C. Gibson,[†,‡,§] Jay Bowman-Kirigin,[†,‡] Lise Sorensen,[†,‡] Jing Ling,[†,‡] Huiming Sun,[†,‡,¶] Sutip Navankasattusas,[†,‡] and Dean Y. Li[†,‡,‖,#,,††]**

The vascular endothelium responds to infection by destabilizing endothelial cell–cell junctions to allow fluid and cells to pass into peripheral tissues, facilitating clearance of infection and tissue repair. During sepsis, endotoxin and other proinflammatory molecules induce excessive vascular leak, which can cause organ dysfunction, shock, and death. Current therapies for sepsis are limited to antibiotics and supportive care, which are often insufficient to reduce morbidity and prevent mortality. Previous attempts at blocking inflammatory cytokine responses in humans proved ineffective at reducing the pathologies associated with sepsis, highlighting the need for a new therapeutic strategy. The small GTPase ARF6 is activated by a MyD88–ARNO interaction to induce vascular leak through disruption of endothelial adherens junctions. In this study, we show that the MyD88–ARNO–ARF6–signaling axis is responsible for LPS-induced endothelial permeability and is a destabilizing convergence point used by multiple inflammatory cues. We also show that blocking ARF6 with a peptide construct of its N terminus is sufficient to reduce vascular leak and enhance survival during endotoxic shock, without inhibiting the host cytokine response. Our data highlight the therapeutic potential of blocking ARF6 and reducing vascular leak for the treatment of inflammatory conditions, such as endotoxemia. ***The Journal of Immunology*****, 2014, 192: 000–000.**

The innate immune system is the first line of defense against pathogenic microbes. It facilitates the recognition of microbial components, such as endotoxin, and initiates an inflammatory response that clears the invading organism and promotes reconstruction of damaged tissues. People with sepsis often have a frenetic inflammatory response and associated excess vascular leak that leads to tissue edema, organ failure, shock, and often death (1–3). Current treatment options are limited to supportive care and antibiotic therapies (4). Unfortunately, even with these options mortality still occurs in >25% of septic patients and occurs with even greater incidence in patients whose condition progresses to septic shock (5, 6).

The vast majority of therapeutic interventions for sepsis, outside of antibiotic therapies and supportive care, have focused on reducing the inflammatory and cytokine responses (7). These approaches, which include immunosuppression by steroids (8), inhibition of the inflammatory TLR4 with eritoran (9), and, in particular, direct inhibition of cytokines, such as TNF-α (10–12), have been successful in some animal models, but they have produced conflicting or negative outcomes in human phase III clinical trials. Because of this, alternative inflammatory pathways important to the pathology of sepsis need to be identified to exploit their potential as therapeutic targets.

The recognition of microbial components by TLRs is critical to the inflammatory response during sepsis. TLRs are expressed in many cell types and stimulate a MyD88-mediated cascade, which leads to activation of the inflammatory transcription factor NF-κB and to the subsequent cytokine storm observed during sepsis (13, 14). We recently identified an association between MyD88 and the guanine nucleotide exchange factor ARNO. IL-1β requires this association to activate ARF6 and to induce vascular leak in a process independent of MyD88's canonical role in NF-κB–mediated inflammatory gene expression (15). This MyD88–ARNO–ARF6 cascade promotes enhanced vascular permeability through the internalization of vascular endothelial-cadherin (VE-cadherin). MyD88 is a critical adapter protein used by numerous other inflammatory pathways, including IL-18R and most of the described TLRs (14). Therefore, we hypothesized that TLR stimulation may induce vascular permeability independent from cytokine expression, that this permeability is mediated by a MyD88–ARNO–ARF6 cascade, and that blocking ARF6 would enhance survival in models of sepsis.

Materials and Methods

Reagents

Human dermal microvascular endothelial cells (HMVEC-Ds) were purchased at passage 0 from Lonza; experiments were performed at passages

*Department of Human Genetics, University of Utah, Salt Lake City, UT 84112; †Program in Molecular Medicine, University of Utah, Salt Lake City, UT 84112; ‡Department of Medicine, University of Utah, Salt Lake City, UT 84112; §Department of Bioengineering, University of Utah, Salt Lake City, UT 84112; ¶Department of Respiratory and Critical Care Medicine, Jinling Hospital, Clinical School of Nanjing University, Nanjing 210002, China; ‖Department of Oncological Sciences, University of Utah, Salt Lake City, UT 84112; #Division of Cardiology, Department of Medicine, University of Utah, Salt Lake City, UT 84112; **The Key Laboratory for Human Disease Gene Study of Sichuan Province, Institute of Laboratory Medicine, Sichuan Academy of Medical Sciences & Sichuan Provincial People's Hospital, Chengdu, Sichuan 610072, China; and ††Cardiology Section, VA Salt Lake City Health Care System, Salt Lake City, UT 84112

Received for publication January 31, 2014. Accepted for publication April 16, 2014.

This work was supported by the National Institutes of Health, the American Heart Association, the H.A. and Edna Benning Foundation, the Juvenile Diabetes Research Foundation, and the Burroughs Wellcome Fund (to D.Y.L.).

C.T.D. and D.Y.L. were responsible for project conceptualization, data analysis, and manuscript preparation. C.T.D., W.Z., C.C.G., J.B.-K., L.S., J.L., H.S., S.N., and D.Y.L. were responsible for assay design and data collection. D.Y.L. was responsible for funding the project.

Address correspondence and reprint requests to Dr. Dean Y. Li, University of Utah, Building 533, Room 4220, 15 N 2030 E, Salt Lake City, UT 84112. E-mail address: dean.li@u2m2.utah.edu

Abbreviations used in this article: DD, death domain; EEA1, early endosome Ag 1; HBSS/A, HBSS supplemented with 1% human serum albumin; HMVEC-D, human dermal microvascular endothelial cell; ID, intermediate domain; PMN, polymorphonuclear leukocyte; siRNA, small interfering RNA; TIR, Toll/IL-1R; VE-cadherin, vascular endothelial cadherin.

3–6. The IKKβ/NF-κB inhibitor, SC-514, was purchased from Calbiochem. The IKK-ε/IRF3 inhibitor, BX-795, was purchased from EMD Millipore. Small interfering RNAs (siRNAs) were purchased from QIAGEN. *Salmonella enterica* serotype enteritidis LPSs were purchased from Sigma: catalog number L7770 was used for in vitro experiments, and catalog number L6011 was used for in vivo experiments. Endothelial cells were cultured in EGM-2MV (Lonza).

siRNAs

siRNAs were diluted in 12.5% by volume HiPerFect Transfection Reagent (QIAGEN) in Opti-MEM (Invitrogen) and incubated for ≥10 min at room temperature. Passage 3–4 endothelial cells were trypsinized, resuspended in growth media, and combined with siRNAs, such that the final concentration of siRNA was 30 nM for all targets. Cells were plated, and media were changed the following morning. Three days after the initial transfection, the cells were transfected a second time using HiPerFect/siRNA concentrations, as described above. All siRNA treatments were compared with the All-Stars Control siRNA (QIAGEN). The catalog numbers and target sequences of siRNAs used throughout this article are as follows: ARF6 (catalog number SI02757286) 5′-CAACGTGGAGACGGTGACTTA-3′; MyD88 (catalog number SI00300909) 5′-AACTGGAACAGACAAACTATC-3′; and ARNO (catalog number SI00061299) 5′-CACGCTGTTGGTAATCTTATT-3′.

Peptide synthesis

Peptides were synthesized in the University of Utah DNA/Peptide Core Facility, using a standard Fmoc synthesis protocol, on an ABI 433 synthesizer (Life Technologies/Applied Biosystems, Carlsbad, CA). In each cycle, a 3- or 4-fold excess of the Fmoc–amino acid was activated with a mix of 2-(1H-benzotriazole-1-yl)-1,1,3,3-tetramethylaminium hexafluorophosphate, Oxyma Pure (ethyl cyano(hydroxyimino)acetate), and diisopropylethylamine (1:1:2). Fmoc was removed in each cycle with 20% piperidine. In peptides with N-terminal myristoyl the last coupling was myristic acid. The peptide was cleaved and deprotected in a 2-h treatment with trifluoroacetic acid/water/triisopropylsilane (95:2.5:2.5), followed by precipitation in diethyl ether. The crude peptides were purified by reversed-phase chromatography using a Hamilton PRP-1 column (Sigma Aldrich) for myristoylated peptides or a Higgins Proto 200 C18 column (Higgins Analytical, Mountain View, CA) for peptides without myristoyl. In either case, a gradient of water/acetonitrile containing 0.1% trifluoroacetic acid was used. The purest fractions of the eluate were combined, lyophilized, redissolved in 0.1 M HCl, and lyophilized again. Final purity was >95%, as measured by reversed-phase chromatography monitored at 214 nm. Molecular mass was confirmed within 0.1 Da by MALDI mass spectrometry. The sequences of the peptides used throughout this article are as follows: MyrARF6 2–13: Myristoyl- GKVLSKIFGNKE; MyrSCR 2–13: Myristoyl- GNFKVILKGKES; and ARF6 2–13: GKVLSKIFGNKE.

Transwell permeability

Permeability assays were adapted from previous protocols (15–17). Twenty-four–well Costar cell culture inserts (1.0 μm pore, 0.3 cm^2 total growth area), coated with 100 μl 15 μg/ml human fibronectin solution, were seeded with 30,000 HMVEC-Ds/insert, for a total of 105 cells/cm^2. The media were replaced the following day, and the assay was performed after a stable confluent monolayer was formed, 48–72 h after seeding. LPS (100 ng/ml) or Mock was added to both apical and basolateral sides of the cell culture insert chamber in phenol red–free media and allowed to stimulate for 4 h. HRP was added at a final concentration of 1 mg/ml to the apical side of the cell culture insert 3 h after stimulation and allowed to leak for 1 h. Media from the lower chamber were collected, and HRP concentration was assessed by the addition of 0.5 mM guaiacol and 0.6 mM H_2O_2. Spectrophotometric analysis of absorbance at 490 nm was used to assess permeability. For assays in which FITC dextran was used as a reporter, the same protocol was followed with two exceptions: the assay was carried out in EGM-2MV, and fluorometric analysis of media in the lower chamber was performed using a microplate fluorometer to assess fluorophore concentration. Data are presented as mean ± SEM of at least three independent experiments and ≥12 individual replicates.

ARF6-activation assay

Primary HMVEC-Ds were treated with agonists and inhibitors, as described in the figure legends. Cells were lysed and immunoprecipitated with GGA3-conjugated agarose beads (Cell Biolabs; STA419). Immunoprecipitates (GTP-bound ARF6) and whole-cell lysates (total ARF6) were analyzed via Western blot with an anti-ARF6 Ab (1:1000; Millipore; 05-1149).

VE-cadherin internalization

Internalization assays were adapted from previous protocols (15, 17). HMVEC-Ds were seeded on eight-well, glass-bottom chamber slides coated with human fibronectin. Cells were incubated in dialyzed VE-cadherin BV6 Ab solution (Millipore; MABT134) that was diluted in labeling buffer (EBM-2 [Lonza] + 3% fatty acid–free BSA + 20 mM HEPES) at a concentration of 5 μg/ml for 1 h at 4°C. Media were replaced with EGM-2MV with 100 ng/ml LPS or vehicle to stimulate endocytosis and 0.6 mM Primaquine (Sigma) to block recycling of vesicles back to the plasma membrane. Cells were acid washed three times in HBSS (Invitrogen) + Ca + Mg + 3% fatty acid–free BSA + 50 mM glycine (pH 2.7) to remove noninternalized Ab and then fixed in 4% paraformaldehyde for 10 min at room temperature. Fixative was washed away with HBSS, and cells were permeabilized with 0.3% Triton in HBSS for 5 min, followed by blocking in 5% nonfat milk + 10% normal donkey serum in HBSS for 1 h. Detection of VE-cadherin was performed with Alexa Fluor 488–conjugated anti-mouse IgG (Invitrogen), and cells were mounted in Antifade medium + 2 μg/ml DAPI. Five random fields/well were imaged on an Olympus FV1000 confocal microscope at 600× with three individual Z-slices, 0.3 μm apart. To quantify the images, each cell with >10 vesicles stained positive for VE-Cadherin was tallied and divided by the total number of DAPI-stained nuclei in the field. To score the image, the total number of cells with greater than 10 488 nm positive vesicles divided by the total number of cells (DAPI-stained nuclei)/field of a collapsed Z-projection was calculated. Statistics were performed, using two-way ANOVA, in Prism software.

Colocalization with EEA1 was performed in the same manner, but the rabbit early endosome Ag 1 (EEA1) primary Ab (Abcam) was added immediately after the blocking step and incubated for 1 h at room temperature.

Immunoprecipitation

The coding sequence of each functional domain of full length of MyD88 and ARNO was amplified from IMAGE cDNA clones by PCR and ligated into pcDNA3.1 vector after enzyme digestion. The ARNO and functional-domain constructs contained a Myc and His epitope, whereas MyD88 constructs contained an HA epitope. 293T cells were transfected with the indicated MyD88 or ARNO constructs. Cells were lysed in ice-cold 50 mM Tris (pH 7.5), 750 mM $MgCl_2$, 1% Nonidet P-40, and 10% glycerol supplemented with protease and phosphatase inhibitors (Thermo; 1861282) and incubated with immobilized anti-HA high-affinity rat mAb (clone 3F10) agarose beads (Roche; 11 815 016 001) for 60 min at 4°C. Complexes were washed three times with lysis buffer and analyzed via Western blot.

Cytokine analysis

HMVEC-D supernatants were treated as described in the figure legends. Cytokine expression was measured with Millipore Milliplex magnetic bead assays, per the manufacturer's instructions. To assess murine plasma TNF-α concentrations, 3–4-mo-old mice that had been treated i.p. with 25 mg/kg LPS and i.v. with 40 mmol/kg peptide or vehicle were anesthetized, and blood was collected via terminal cardiac puncture in the presence of EDTA. Whole blood was centrifuged, and the plasma was obtained and stored at −80°C until analysis. TNF-α concentrations were analyzed using the Mouse TNF-α DuoSet ELISA (R&D Systems; DY410).

Leukocyte rolling and adherence assay

The protocol was adapted from previous studies (18, 19). HMVEC-Ds were seeded into each well of a human fibronectin–coated parallel plate flow chamber (U-plate 0.4 VI Fibronectin; Ibidi) at a density of 3×10^4 cells/chamber. Media were changed daily until the cells had grown to confluence.

Human polymorphonuclear leukocytes (PMNs) were isolated using previously described protocols (20, 21). Human peripheral venous blood was collected from healthy, medication-free adult subjects and drawn into acid-citrate-dextrose (14% final concentration) through standard venipuncture technique and used immediately upon collection. All subjects provided informed consent, and Institutional Review board approval was received for blood collection at the University of Utah. Platelet-rich plasma was removed upon centrifugation of whole blood at $150 \times g$ for 20 min at room temperature. The remaining red/WBC mixture was resuspended back to the original volume with 0.9% saline solution. Six percent dextran 70 was added to the cell mixture and left for 1 h. The leukocyte-rich supernatant was removed and centrifuged at $400 \times g$ for 5 min at 4°C. The supernatant was discarded, and the pellet was resuspended in 0.2% NaCl immediately followed with an equal part 1.6% NaCl. Cells were centrifuged

at 400 × *g* for 5 min at 4°C. The pellet was resuspended in HBSS supplemented with 1% human serum albumin (HBSS/A) and layered over an equal volume of Ficoll-Paque Plus. The suspension was centrifuged at 4°C for 30 min at 400 × *g*. The mononuclear leukocyte layer was removed, followed by the RBC layer, HBSS/A layer, and Ficoll-Paque layer. The remaining pellet containing ≥95% PMNs was washed with HBSS/A and resuspended to 10^6 cells/ml in warm Ultrasaline.

Endothelial cells previously seeded into flow chambers were treated with LPS (100 ng/ml) and/or SC-514 for 3 h in complete media. A syringe pump (Harvard Apparatus) was used to propel isolated and unstimulated primary human leukocytes through the parallel plate flow chambers (at 1 dyne × cm^{-1} [typical venous shear stress (22)]) in Ultrasaline. Differential interference contrast microscopy images were taken one time per second for 30 s using an Olympus inverted microscope and a 10× objective, which is sufficient for visualizing a large number of endothelial cells. The imaged area was in the center (in both length and width) of each well, a point confirmed by the manufacturer using computational fluid dynamics to demonstrate the most uniform flow characteristics. The total number of PMNs rolling and adhered in all 30 images was quantified using MetaMorph software. Data presented are a quantification of the cumulative number of cells observed to be adhered or rolling on the endothelial monolayer in each image (total leukocytes adhered/30 s) ± SEM and are representative of one large field of view in the center of the well from at least four independent replicates. Statistics were calculated using ANOVA and the Dunnett multiple-comparison post hoc test.

VE-cadherin area quantification

HMVEC-Ds were seeded on BD Falcon clear-bottom 96-well tissue culture plates (catalog number 353219) at a density of 10,000 cells/well. Cells were incubated with the indicated treatments for 5 h and then fixed with 4% paraformaldehyde in PBS for 10 min. Cells were permeabilized with 0.5% Triton-X 100 for 2 min, blocked with Odyssey Blocking Buffer (LI-COR Biosciences) for 30 min at room temperature, and incubated with a mouse monoclonal VE-Cadherin Ab (BD; 555661) overnight at 4°C. Cells were rinsed with PBS and incubated with Alexa Fluor 488 donkey anti-mouse secondary Ab and Hoechst 33258 dye for 4 h at room temperature. Cells were rinsed, and the ImageXpress Micro XLS (Molecular Devices) collected nine nonoverlapping images at the center of each well with a 20× objective. The VE-cadherin area of each image was quantified with ImageJ by batch thresholding all images from an individual experiment and quantifying the number of pixels that were VE-cadherin$^+$ within each image. The VE-cadherin area was divided by the number of nuclei/image and normalized to the Mock treatments. Data were compiled from three independent experiments with three replicate wells/condition in each experiment and are composed of nine images/well, for a total of 81 images/condition.

Organ permeability

This assay was adapted from previously published protocols (1, 23, 24). Male C57BL/6 mice, between 8 and 12 wk of age (The Jackson Laboratory) were anesthetized with ketamine and given 40 mmol/kg peptide, followed by 40 mg/kg Evans Blue dye in saline delivered i.v. via retro-orbital sinus injection. Anesthesia was reversed with 50 μl 500 μg/ml Antisedan (atipamezole) administered s.c. Six hours later, mice were euthanized via CO_2 asphyxiation, and the mass of each organ was measured. Organs were placed in 1 ml formamide for 72 h at 60°C to elute the dye from each organ. Organs were centrifuged, and Evans blue dye accumulation was measured at 620 nm with 740 nm correction. Values were compared with a standard curve to calculate the total amount of dye/g (wet-weight) in each organ. All animal experiments were approved by the Animal Care and Use Committee of the University of Utah under protocol number 12-10002.

Endotoxemia survival

Eight- to twelve-week-old male C57BL/6 mice (The Jackson Laboratory), given 40 mmol/kg peptide i.v. via retro-orbital sinus injection and 25 mg/kg of LPS i.p., were monitored at least four times each day until all living mice resumed normal behaviors. To reduce death as an end point, all mice observed to be unresponsive to touch were euthanized immediately by CO_2 asphyxiation.

Statistics

Unless otherwise noted, statistics and *p* values were calculated using one-way ANOVA, with the appropriate post hoc test, in PRISM software version 5.0f.

Results

TLRs induce vascular leak by activation of ARF6

To determine whether ARF6 is involved in TLR-mediated endothelial permeability, we used a well-characterized endothelial cell,

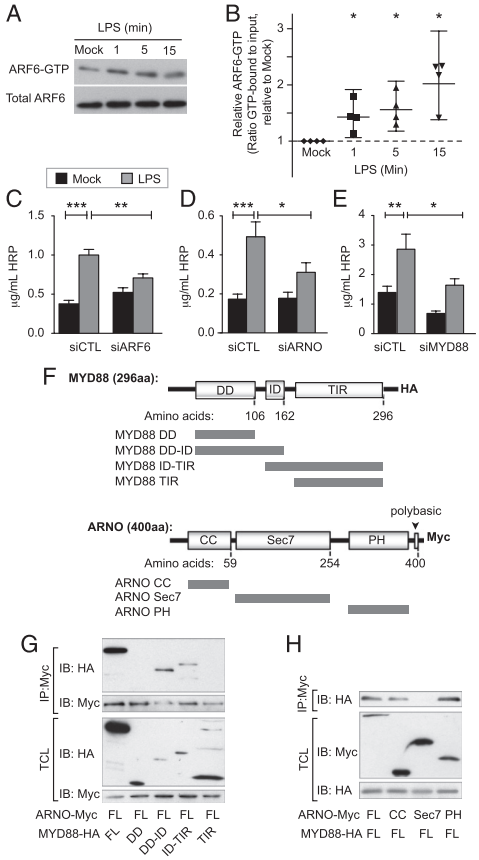

FIGURE 1. LPS uses the MyD88–ARNO–ARF6 cascade to destabilize endothelial barriers. (**A**) HMVEC-Ds were exposed to 100 ng/ml LPS, and active, GTP-bound ARF6 was assessed by GGA3 immunoprecipitation assay and compared with total ARF6 in the lysate. (**B**) Quantification of data in (A) showing the geometric mean and 95% confidence interval; asterisks denote statistically significant results for which the lower bound of the 95% confidence interval for the normalized ratio does not cross 1 (the null value, represented as a dashed line). (**C**) HMVEC-Ds treated with siRNAs directed toward ARF6 or a nontargeting control RNA (siCTL) were assessed for their ability to reduce the leak of an HRP reporter after treatment with 100 ng/ml LPS. HMVEC-Ds were transfected with siRNAs targeting ARNO (**D**) or MyD88 (**E**) and assessed for the flow of HRP across an endothelial monolayer after exposure to 100 ng/ml LPS. One-way ANOVA, with Dunnett multiple-comparison test, were used for statistical analysis. (**F**) Domain map of MyD88 and ARNO constructs. (**G**) Lysates from HEK 293T cells expressing ARNO-Myc and the indicated MyD88-HA constructs were immunoprecipitated with anti-Myc Abs and immunoblotted with anti-HA Abs. (**H**) Lysates from HEK 293T cells expressing MyD88-HA and the indicated ARNO-Myc constructs were immunoprecipitated with anti-Myc Abs and immunoblotted with anti-HA Abs. $*p < 0.05$, $**p < 0.01$, $***p < 0.001$.

found to be sufficient for ARNO's interaction with MyD88 (Fig. 1G, 1H).

A MyD88–ARNO–ARF6–controlled permeability hypothesis suggests that, like IL-1β, modulation of ARF6 may be independent of LPS-induced changes in gene expression and that those changes may be dispensable for LPS-induced permeability. Indeed, siRNAs targeting ARF6 were unable to block LPS-induced TNF-α expression in endothelial cells (Fig. 2A). Additionally, blocking LPS-induced transcription factor NF-κB or IRF3 activation using SC-514 or BX-795, respectively, failed to inhibit LPS-induced permeability, but it blocked other LPS-induced responses, including leukocyte rolling and TNF-α and IL-6 expression (Fig. 2B–F) (33, 34).

LPS induces permeability through VE-cadherin disruption

ARF6 was implicated in the regulation of the internalization of the adherens junction protein VE-cadherin, which suggests that the LPS-mediated increase in endothelial permeability occurs in a paracellular manner. To test this, we assessed the leak of 2-MDa FITC-dextran, a reporter too large for transcellular transport across endothelial monolayers (35). We observed enhanced movement of the 2-MDa dextran across the monolayer upon LPS stimulation, suggesting that LPS enhances paracellular leak across the endothelium (Fig. 3A). LPS also induced VE-cadherin internalization, as shown by the enhanced presence of VE-cadherin in endocytic vesicles containing EEA1 (Fig. 3B–D). This internalization was abolished upon treatment of endothelial cells with siRNA directed against ARF6 mRNA, further supporting the hypothesis that LPS mediates permeability through ARF6-mediated adherens junction internalization (Fig. 3E, 3F).

Inhibition of ARF6 with its N terminus reduces vascular leak

Having established that activation of ARF6 plays a critical role in the enhancement of endothelial permeability, we wanted to determine whether deactivation of ARF6 would enhance endothelial barriers and reduce leak. A property of the ARF family of GTPases is that peptides constructed of their N termini are proposed to inhibit ARF GDP–GTP exchange (36, 37). We synthesized a myristoylated peptide composed of amino acids 2–13 of ARF6 (MyrARF6 2–13). The ARF6 N-terminal peptide, but not scrambled (MyrSCR 2–13) or nonmyristoylated (ARF6 2–13) controls, was sufficient to reduce ARF6 activation in HMVEC-Ds (Fig. 4A, 4B).

Our model predicts that reduced ARF6 activation would result in enhanced endothelial barrier function. The ARF6 N terminus, but not nonmyristoylated or scrambled controls, reduced permeability across an endothelial monolayer (Fig. 4C). This reduction in permeability corresponded to an increase in VE-cadherin at cell junctions (Fig. 4D, 4E). This ARF6 inhibitory function was also active in vivo and prevented the leak of Evans Blue dye from the blood into both the lungs and the kidneys (Fig. 4F, 4G). These data suggest that the synthetic ARF6 N terminus may be useful as a novel therapeutic to prevent pathologies resulting from excess inflammatory vascular leak.

The synthetic N terminus of ARF6 enhances survival during endotoxic shock

Sepsis is a condition characterized by immense vascular leak that leads to tissue dysfunction, shock, and, eventually, death. We sought to determine whether the stabilizing activity of the ARF6 N terminus could enhance survival of mice in the endotoxemia model of sepsis. Lethal doses of LPS were administered i.p. immediately following i.v. injection of peptides. Mice were monitored at least four times per day until they resumed normal grooming behaviors for ≥24 h. After 48 h, only 20% of the mice treated with LPS plus

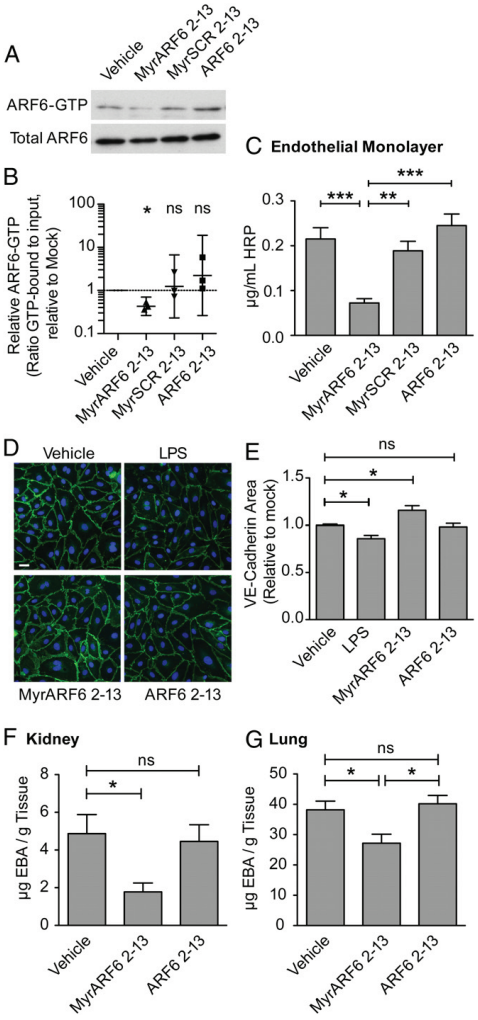

FIGURE 4. An N terminus ARF6 peptide inhibits ARF6 activation and reduces vascular permeability. (**A** and **B**) HMVEC-Ds were exposed to 25 μM of the myristoylated ARF6 2–13 peptide, nonmyristoylated ARF6 2–13 peptide, scrambled myristoylated ARF6 2–13 peptide, or vehicle, and lysates were assessed for the ratio of ARF6-GTP/total ARF6 in the cell lysates. Data are geometric mean and 95% confidence interval; asterisk denotes a statistically significant result in which the upper bound of the 95% confidence interval for the normalized ratio does not cross 1 (the null value, represented as a dashed line). HMVEC-Ds were exposed to the indicated treatments and assessed for their ability to inhibit leak of HRP (**C**) or increase VE-cadherin surface area (**D** and **E**). Mice were administered 40 mmol/kg of the indicated peptides i.v. with Evans Blue dye. Kidneys (**F**) and lungs (**G**) were removed 6 h postinjection. The concentration of dye in each tissue is shown. Representative panels in (D) were selected after enhancement of contrast to 0.4% saturation of pixels. Scale bar, 30 μm. $*p < 0.05$, $**p < 0.01$, $***p < 0.001$, one-way ANOVA and Tukey multiple-comparison test. ns, not significant.

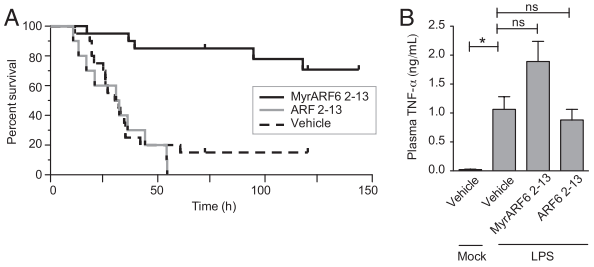

FIGURE 5. The synthetic ARF6 N-terminal peptide enhances survival during endotoxemia. Mice were anesthetized with ketamine and administered a lethal dose (25 mg/kg) of LPS i.p. concurrently with 40 mmol/kg the indicated peptide i.v. and monitored for survival (**A**) and plasma TNF-α concentration after 5 h ($n = 4$ mice/group) (**B**). *$p < 0.05$, Mantel–Cox test (A) and one-way ANOVA with Dunnett multiple-comparison test (B). ns, not significant.

vehicle or a nonmyristoylated peptide were alive. However, 85% of the mice treated with LPS plus ARF6 N-terminal peptide were alive at 48 h, and >70% of the mice recovered completely (Fig. 5A). Interestingly, peptide treatment enhanced survival but did not significantly affect serum cytokine levels (Fig. 5B). The observation that peptide treatment does not affect cytokine levels provides further evidence that ARF6 pathway inhibition can protect mice from the deleterious effects of inflammation while allowing canonical inflammatory cascades to continue (Fig. 6).

Discussion

We defined a signaling cascade in endothelial cells by which LPSs induce vascular leak. We also described a peptide inhibitor of this pathway, MyrARF6 2–13, which stabilized the vasculature in both in vitro and in vivo assays and enhanced survival in a mouse model of endotoxic shock.

The endothelial cell monolayer is the critical barrier between blood and the peripheral tissues. It regulates the migration of fluid, nutrients, and cells from blood into the interstitial space. The integrity of this barrier is maintained by a balance of opposing cues that regulate endothelial cell transcytosis and cell–cell junctions (38). For example, homophilic interactions of VE-cadherin at the cell–cell junction are enhanced upon stimulation by TIE2-dependent angiopoietin signaling (39) and ROBO4-dependent SLIT signaling (1), but they are disrupted after stimulation with destabilizing cues, such as VEGF (17), IL-1β (15), or LPS, as described in this article. The ability of the stabilizing receptor ROBO4 to prevent leak and pathologic angiogenesis is dependent on its ability to recruit the GTPase activating protein, GIT1, to inactivate ARF6 (40). Conversely, the ability of the inflammatory mediators LPS and IL-1β to destabilize the vasculature is dependent on their ability to activate ARF6 (15). These observations, combined with the data from this study, place ARF6 at the nexus of multiple pathways that disrupt the endothelium. ARF6 activation leads to an unstable, leaky vasculature, whereas ARF6 inhibition leads to a stable, less permeable vasculature. This tightly regulated balance of endothelial stability is disrupted in conditions such as sepsis or pulmonary infections. During these conditions, the inflammatory response induces intractable vascular leak, hypovolemic shock, and/or acute respiratory distress syndrome, all of which can precipitate death. By blocking ARF6 with its N-terminal peptide and reducing vascular leak, we were able to enhance the survival of mice in the endotoxemia model of sepsis.

Our in vitro and in vivo data demonstrate that ARF6 regulates permeability independent from downstream inflammatory gene expression. Knockdown of *ARF6* expression in endothelial cells, using specific siRNAs and the systemic in vivo administration of the ARF6 N-terminal peptide, did not block LPS-induced TNF-α secretion. Thus far, all of the evidence in animal models, including the current study, suggests that ARF6, although necessary for disease pathology, does not regulate cytokine release (15). In contrast, it was proposed that inhibition of ARF6 in fibroblasts, macrophages, and dendritic cells decreases LPS-induced cytokine production by preventing the association of MyD88 with TIRAP and TLR4 (41, 42). However, LTA-induced cytokine expression, which also requires the association of MyD88 with TIRAP, was not affected by ARF6 inhibition, suggesting a greater complexity in these TLR-signaling pathways (42). Furthermore, ARF6 inhibition had no effect on LPS-induced cytokine expression in dendritic cells (43). Therefore, the preponderance of in vitro evidence, as well as that from all in vivo studies published to date, suggests that ARF6 inhibition does not block cytokine expression or release.

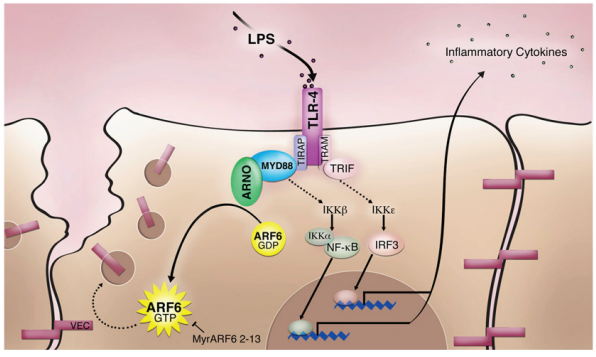

FIGURE 6. LPS uses a MyD88–ARNO–ARF6 cascade to induce VE-cadherin internalization and vascular permeability independent from cytokine expression. LPS stimulates TLR4, which recruits the adapter proteins MyD88 and TRIF to facilitate downstream transcriptional regulation, such as cytokine expression. LPS also stimulates an independent and divergent pathway through the MyD88–ARNO–ARF6–signaling axis that dissociates VE-cadherin from the cell–cell junctions, allowing for vascular leak to occur. MyrARF6 2–13 blocks this divergent pathway by deactivating ARF6 and reducing vascular leak.

Aside from enhancing vascular stability, inhibition of a highly conserved molecule, such as ARF6, may have a number of developmental effects. For example, genetic ablation of ARF6 leads to the failure of proper hepatic cord formation and is embryonically lethal (44). However, the specific ablation of ARF6 in adults has not been described. In adult mice, inhibition of the ARF family of GTPases prevented signal transduction of the insulin-receptor complex, leading to transient insulin resistance (45). Additionally, inhibition for 2 wk showed no obvious toxicity, but it decreased inflammatory pathologies in mouse models of arthritis (15). ARF inhibition also reduced invasion and metastasis of melanoma xenografts (31). Furthermore, ARF6 inhibition blocked proper VEGF receptor signaling and angiogenesis (40, 46), as well as altered platelet activation (36, 47). Determining the effects of ARF6 inhibition on other tissues, especially in the context of hyperinflammation and sepsis, is an important and ongoing area of research in our laboratory and others.

This study identified a novel host–pathogen interaction through which bacterial LPSs activate a MyD88–ARNO–ARF6 cascade that induces endothelial leak independent of cytokine expression after stimulation (Fig. 6). We characterize an ARF6 inhibitor that reduces vascular leak and increases survival during lethal LPS-induced endotoxemia. MyD88 is a central effector of innate immunity; blocking the MyD88–ARNO–ARF6 cascade might serve to stabilize the vasculature and prevent pathologies induced by multiple diverse inflammatory events, regardless of the stimulus. We expect that this study will open new avenues for the development of therapeutics that could be used for the treatment of inflammatory processes related to infection, as well as any inflammatory process associated with vascular instability, including trauma, epilepsy, and autoimmune diseases, such as multiple sclerosis (48–50).

Acknowledgments

We thank S. Odelberg, K. Thomas, A. Chan, N. London, R. Campbell, and G. Zimmerman for critical reading and experimental advice; K. Onstanin, R. A. Kahn, and P. Randazzo for experimental advice and guidance; T. Mleynek for technical and graphical assistance; and the University of Utah Microscopy, Phenotyping, and Animal Cores for technical assistance. We especially thank Scott Endicott (University of Utah DNA/Peptide Core Facility) for peptide synthesis. We thank Chi Yen for technical assistance with cytokine arrays.

Disclosures

D.Y.L. and the University of Utah own intellectual property regarding the use of ARF6 inhibitors.

References

1. London, N. R., W. Zhu, F. A. Bozza, M. C. Smith, D. M. Greif, L. K. Sorensen, L. Chen, Y. Kaminoh, A. C. Chan, S. F. Passi, et al. 2010. Targeting Robo4-Dependent Slit Signaling to Survive the Cytokine Storm in Sepsis and Influenza. *Sci. Transl. Med.* 2: 23ra19.
2. Cohen, J. 2002. The immunopathogenesis of sepsis. *Nature* 420: 885–891.
3. Lee, W. L., and A. S. Slutsky. 2010. Sepsis and endothelial permeability. *N. Engl. J. Med.* 363: 689–691.
4. Dellinger, R. P., M. M. Levy, A. Rhodes, D. Annane, H. Gerlach, S. M. Opal, J. E. Sevransky, C. L. Sprung, I. S. Douglas, R. Jaeschke, et al; Surviving Sepsis Campaign Guidelines Committee including The Pediatric Subgroup. 2013. Surviving Sepsis Campaign: international guidelines for management of severe sepsis and septic shock, 2012. *Intensive Care Med.* 39: 165–228.
5. Annane, D., P. Aegerter, M. C. Jars-Guincestre, and B. Guidet; CUB-Réa Network. 2003. Current epidemiology of septic shock: the CUB-Réa Network. *Am. J. Respir. Crit. Care Med.* 168: 165–172.
6. Angus, D. C., and T. van der Poll. 2013. Severe sepsis and septic shock. *N. Engl. J. Med.* 369: 840–851.
7. Riedemann, N. C., R. F. Guo, and P. A. Ward. 2003. Novel strategies for the treatment of sepsis. *Nat. Med.* 9: 517–524.
8. Annane, D. 2011. Corticosteroids for severe sepsis: an evidence-based guide for physicians. *Ann. Intensive care* 1: 7.
9. Opal, S. M., P. F. Laterre, B. Francois, S. P. LaRosa, D. C. Angus, J. P. Mira, X. Wittebole, T. Dugernier, D. Perrotin, M. Tidswell, et al; ACCESS Study Group. 2013. Effect of eritoran, an antagonist of MD2-TLR4, on mortality in patients with severe sepsis: the ACCESS randomized trial. *JAMA* 309: 1154–1162.
10. Reinhart, K., and W. Karzai. 2001. Anti-tumor necrosis factor therapy in sepsis: update on clinical trials and lessons learned. *Crit. Care Med.* 29(7, Suppl.)S121–S125.
11. Opal, S. M., C. J. Fischer, Jr., J. F. Dhainaut, J. L. Vincent, R. Brase, S. F. Lowry, J. C. Sadoff, G. J. Slotman, H. Levy, R. A. Balk, et al 1997. Confirmatory interleukin-1 receptor antagonist trial in severe sepsis: a phase III, randomized, double-blind, placebo-controlled, multicenter trial. The Interleukin-1 Receptor Antagonist Sepsis Investigator Group. *Crit. Care Med.* 25: 1115–1124.
12. Tracey, K. J., Y. Fong, D. G. Hesse, K. R. Manogue, A. T. Lee, G. C. Kuo, S. F. Lowry, and A. Cerami. 1987. Anti-cachectin/TNF monoclonal antibodies prevent septic shock during lethal bacteraemia. *Nature* 330: 662–664.
13. van der Poll, T., and S. M. Opal. 2008. Host-pathogen interactions in sepsis. *Lancet Infect. Dis.* 8: 32–43.
14. Warner, N., and G. Núñez. 2013. MyD88: a critical adaptor protein in innate immunity signal transduction. *J. Immunol.* 190: 3–4.
15. Zhu, W., N. R. London, C. C. Gibson, C. T. Davis, Z. Tong, L. K. Sorensen, D. S. Shi, J. Guo, M. C. Smith, A. H. Grossmann, et al. 2012. Interleukin receptor activates a MYD88-ARNO-ARF6 cascade to disrupt vascular stability. *Nature* 492: 252–255.
16. Martins-Green, M., M. Petreaca, and M. Yao. 2008. An assay system for in vitro detection of permeability in human "endothelium." *Methods Enzymol.* 443: 137–153.
17. Gavard, J., and J. S. Gutkind. 2006. VEGF controls endothelial-cell permeability by promoting the beta-arrestin-dependent endocytosis of VE-cadherin. *Nat. Cell Biol.* 8: 1223–1234.
18. Moake, J. L., N. A. Turner, N. A. Stathopoulos, L. Nolasco, and J. D. Hellums. 1988. Shear-induced platelet aggregation can be mediated by vWF released from platelets, as well as by exogenous large or unusually large vWF multimers, requires adenosine diphosphate, and is resistant to aspirin. *Blood* 71: 1366–1374.
19. Wilson, B. D., C. C. Gibson, L. K. Sorensen, M. Y. Guilhermier, M. Clinger, L. L. Kelley, Y.-T. E. Shiu, and D. Y. Li. 2011. Novel approach for endothelializing vascular devices: understanding and exploiting elastin-endothelial interactions. *Ann. Biomed. Eng.* 39: 337–346.
20. Zimmerman, G. A., T. M. McIntyre, and S. M. Prescott. 1985. Thrombin stimulates the adherence of neutrophils to human endothelial cells in vitro. *J. Clin. Invest.* 76: 2235–2246.
21. Yost, C. C., M. M. Denis, S. Lindemann, F. J. Rubner, G. K. Marathe, M. Buerke, T. M. McIntyre, A. S. Weyrich, and G. A. Zimmerman. 2004. Activated polymorphonuclear leukocytes rapidly synthesize retinoic acid receptor-alpha: a mechanism for translational control of transcriptional events. *J. Exp. Med.* 200: 671–680.
22. Milnor, W. R. 1982. *Hemodynamics.* Williams and Wilkins, Baltimore.
23. Radu, M., and J. Chernoff. 2013. An in vivo assay to test blood vessel permeability. J. Vis. Exp. 16: e50062.
24. Han, E. D., R. C. MacFarlane, A. N. Mulligan, J. Scafidi, and A. E. Davis, III. 2002. Increased vascular permeability in C1 inhibitor-deficient mice mediated by the bradykinin type 2 receptor. *J. Clin. Invest.* 109: 1057–1063.
25. Adam, A. P., A. L. Sharenko, K. Pumiglia, and P. A. Vincent. 2010. Src-induced tyrosine phosphorylation of VE-cadherin is not sufficient to decrease barrier function of endothelial monolayers. *J. Biol. Chem.* 285: 7045–7055.
26. Fitzner, N., S. Clauberg, F. Essmann, J. Liebmann, and V. Kolb-Bachofen. 2008. Human skin endothelial cells can express all 10 TLR genes and respond to respective ligands. *Clin. Vaccine Immunol.* 15: 138–146.
27. Zhao, H., A. R. Anand, and R. K. Ganju. 2014. Slit2-Robo4 pathway modulates lipopolysaccharide-induced endothelial inflammation and its expression is dysregulated during endotoxemia. *J. Immunol.* 192: 385–393.
28. Faure, E., O. Equils, P. A. Sieling, L. Thomas, F. X. Zhang, C. J. Kirschning, N. Polentarutti, M. Muzio, and M. Arditi. 2000. Bacterial lipopolysaccharide activates NF-kappaB through toll-like receptor 4 (TLR-4) in cultured human dermal endothelial cells. Differential expression of TLR-4 and TLR-2 in endothelial cells. *J. Biol. Chem.* 275: 11058–11063.
29. El Azreq, M.-A., V. Garceau, D. Harbour, C. Pivot-Pajot, and S. G. Bourgoin. 2010. Cytohesin-1 regulates the Arf6-phospholipase D signaling axis in human neutrophils: impact on superoxide anion production and secretion. *J. Immunol.* 184: 637–649.
30. Morishige, M., S. Hashimoto, E. Ogawa, Y. Toda, H. Kotani, M. Hirose, S. Wei, A. Hashimoto, A. Yamada, H. Yano, et al. 2008. GEP100 links epidermal growth factor receptor signalling to Arf6 activation to induce breast cancer invasion. *Nat. Cell Biol.* 10: 85–92.
31. Grossmann, A. H., J. H. Yoo, J. Clancy, L. K. Sorensen, A. Sedgwick, Z. Tong, K. Ostanin, A. Rogers, K. F. Grossmann, S. R. Tripp, et al. 2013. The small GTPase ARF6 stimulates β-catenin transcriptional activity during WNT5A-mediated melanoma invasion and metastasis. *Sci. Signal.* 6: ra14.
32. Janssens, S., and R. Beyaert. 2002. A universal role for MyD88 in TLR/IL-1R-mediated signaling. *Trends Biochem. Sci.* 27: 474–482.
33. Clark, K., L. Plater, M. Peggie, and P. Cohen. 2009. Use of the pharmacological inhibitor BX795 to study the regulation and physiological roles of TBK1 and IkappaB kinase epsilon: a distinct upstream kinase mediates Ser-172 phosphorylation and activation. *J. Biol. Chem.* 284: 14136–14146.
34. Kishore, N., C. Sommers, S. Mathialagan, J. Guzova, M. Yao, S. Hauser, K. Huynh, S. Bonar, C. Mielke, L. Albee, et al. 2003. A selective IKK-2 inhibitor blocks NF-kappa B-dependent gene expression in interleukin-1 beta-stimulated synovial fibroblasts. *J. Biol. Chem.* 278: 32861–32871.
35. Mehta, D., and A. B. Malik. 2006. Signaling mechanisms regulating endothelial permeability. *Physiol. Rev.* 86: 279–367.

36. Choi, W., Z. A. Karim, and S. W. Whiteheart. 2006. Arf6 plays an early role in platelet activation by collagen and convulxin. *Blood* 107: 3145–3152.
37. Randazzo, P. A., T. Terui, S. Sturch, H. M. Fales, A. G. Ferrige, and R. A. Kahn. 1995. The myristoylated amino terminus of ADP-ribosylation factor 1 is a phospholipid- and GTP-sensitive switch. *J. Biol. Chem.* 270: 14809–14815.
38. Komarova, Y., and A. B. Malik. 2010. Regulation of endothelial permeability via paracellular and transcellular transport pathways. *Annu. Rev. Physiol.* 72: 463–493.
39. Gavard, J., V. Patel, and J. S. Gutkind. 2008. Angiopoietin-1 prevents VEGF-induced endothelial permeability by sequestering Src through mDia. *Dev. Cell* 14: 25–36.
40. Jones, C. A., N. Nishiya, N. R. London, W. Zhu, L. K. Sorensen, A. C. Chan, C. J. Lim, H. Chen, Q. Zhang, P. G. Schultz, et al. 2009. Slit2-Robo4 signalling promotes vascular stability by blocking Arf6 activity. *Nat. Cell Biol.* 11: 1325–1331.
41. Kagan, J. C., and R. Medzhitov. 2006. Phosphoinositide-mediated adaptor recruitment controls Toll-like receptor signaling. *Cell* 125: 943–955.
42. Van Acker, T., S. Eyckerman, L. Vande Walle, S. Gerlo, M. Goethals, M. Lamkanfi, C. Bovijn, J. Tavernier, and F. Peelman. 2014. The small GTPase Arf6 is essential for the Tram/Trif pathway in TLR4 signaling. *J. Biol. Chem.* 17: 1364–1376.
43. Svensson, H. G., M. A. West, P. Mollahan, A. R. Prescott, R. Zaru, and C. Watts. 2008. A role for ARF6 in dendritic cell podosome formation and migration. *Eur. J. Immunol.* 38: 818–828.
44. Suzuki, T., Y. Kanai, T. Hara, J. Sasaki, T. Sasaki, M. Kohara, T. Maehama, C. Taya, H. Shitara, H. Yonekawa, et al. 2006. Crucial role of the small GTPase ARF6 in hepatic cord formation during liver development. *Mol. Cell. Biol.* 26: 6149–6156.
45. Hafner, M., A. Schmitz, I. Grüne, S. G. Srivatsan, B. Paul, W. Kolanus, T. Quast, E. Kremmer, I. Bauer, and M. Famulok. 2006. Inhibition of cytohesins by SecinH3 leads to hepatic insulin resistance. *Nature* 444: 941–944.
46. Hashimoto, A., S. Hashimoto, R. Ando, K. Noda, E. Ogawa, H. Kotani, M. Hirose, T. Menju, M. Morishige, T. Manabe, et al. 2011. GEP100-Arf6-AMAP1-cortactin pathway frequently used in cancer invasion is activated by VEGFR2 to promote angiogenesis. *PLoS ONE* 6: e23359.
47. Kanamarlapudi, V., S. E. Owens, K. Saha, R. J. Pope, and S. J. Mundell. 2012. ARF6-dependent regulation of P2Y receptor traffic and function in human platelets. *PLoS ONE* 7: e43532.
48. Chodobski, A., B. J. Zink, and J. Szmydynger-Chodobska. 2010. Blood-brain barrier pathophysiology in traumatic brain injury. *Transl. Stroke Res.* 2: 492-516.
49. van Vliet, E. A., S. da Costa Araújo, S. Redeker, R. van Schaik, E. Aronica, and J. A. Gorter. 2007. Blood-brain barrier leakage may lead to progression of temporal lobe epilepsy. *Brain* 130: 521–534.
50. Minagar, A., and J. S. Alexander. 2003. Blood-brain barrier disruption in multiple sclerosis. *Mult. Scler.* 9: 540–549.

Appendix: The N-terminus of ARF6 is an antimicrobial peptide with activity *in vitro* but not live animal assays.

Introduction

Thus far, Chapter 3 has demonstrated that a peptide composed of the amino terminus of ARF6 (MyrARF6 2-13) is a potent bioactive molecule that deactivates ARF6 in the endothelium and enhances vascular stability. However, the structure of MyrARF6 2-13 suggests that it may have other functions as well. MyrARF6 2-13 is a cationic, amphipathic helix [1], a trait possessed by a class of peptides functionally named "antimicrobial peptides [2]," or AMPs. The experiments outlined in this appendix characterize MyrARF6 2-13's function as a putative AMP. Our data suggest that MyrARF6 2-13 interacts with LPS, prevents LPS-mediated cytokine production, and inhibits growth of a pathogenic strain of *Escherichia coli* in *in vitro* assays. However, when MyrARF6 2-13 is administered to mice, no such antimicrobial affect was observed, suggesting that its antimicrobial capabilities are limited to *in vitro* settings.

AMPs are a subclass of membrane-active peptides (MAPs) utilized to bind cell-wall components of bacteria and facilitate bacterial lysis. AMPs are similar to another subclass of MAPs known as cell-penetrating peptides used to deliver macromolecules into cells [2b]. One structural domain present in both peptide subclasses is the amphipathic helix. The ARF6 amino terminus (Figure 3.1), the domain of ARF6 responsible for its membrane association, is an amphipathic helix that resembles an antimicrobial peptide [3].

Results

Due to the structural similarly of the ARF6 N-terminus to antimicrobial peptides, we wanted to determine if MyrARF6 2-13 had antimicrobial peptide-like activity. We utilized a cadaverine displacement assay to detect an LPS interaction [4]. BODIPY cadaverine binds to the lipid-A portion of LPS and the resulting hydrophobic environment limits the fluorescence of the BODIPY fluor. In the presence of LPS-binding molecules such as Polymyxin B or antimicrobial peptides, the bodipy cadaverine is released and fluorescence is enhanced. Indeed, presence of both L- and D-enantiomers of MyrARF6 2-13, but not scrambled (MyrSCR 2-13) or non-myristoylated controls, were sufficient to enhance the fluorescence of bodipy cadaverine in the presence of LPS, suggesting that MyrARF6 2-13 can bind and interact with LPS and this interaction is chirality-independent.

Having detected a potential interaction between MyrARF6 2-13 and LPS, we sought to determine if MyrARF6 2-13 could prevent LPS-induced signal transduction. Upon treatment with LPS, endothelial cells secrete cytokines into the culture media. If MyrARF6 2-13 prevents LPS-mediated signal transduction, we would expect a reduction in the total amount of cytokines released into the culture media. Indeed, both L- and D-enantiomers of MyrARF6 2-13 were sufficient to block LPS-mediated IL-6 secretion, but not TNF-α-mediated IL-6 secretion (Figure 3.3).

Many LPS-binding peptides not only prevent LPS-induced signaling cascades, but are bactericidal and prevent bacterial replication [2a]. Because of this, we wanted to determine if MyrARF6 2-13 was bactericidal. Indeed, both enantiomers of MyrARF6 2-13 equally blocked the growth of *E. coli*, but not to the same potency as previously

described antimicrobial molecules: Temporin L and Polymyxin B (Table 3.1). Collectively, our data suggest that the N-terminus of ARF6 has antimicrobial activity and could be classified as an AMP.

Having determined that both L- and D- enantiomers of MyrARF6 were equipotent antimicrobial peptides, it became necessary to determine the contribution of the peptide's antimicrobial activity to the enhancement of survival during endotoxemia we observed in the published work, in figure 5 of J. Immun 16 May, 2014, doi:10.4049/jimmunol.1400309. We hypothesized that it would be unlikely for the D-enantiomer of MyrARF6 2-13 have the same ability to deactivate endogenous ARF6 and enhance endothelial stability as the L-enantiomer. Although both enantiomers display equipotent antimicrobial activities, the D-enantiomer is unable to deactivate endothelial ARF6 or enhance endothelial barrier function to the same extent as the L-enantiomer (Figure 3.4).

Having observed that L-MyrARF6 2-13 behaves as an antimicrobial peptide that also inhibits ARF6 signaling and enhances endothelial stability, and the D-enantiomer only has antimicrobial activity, we were able to use the D-enantiomer to experimentally control for the antimicrobial activity of the L-enantiomer during endotoxemia. We therefore assessed the survival of mice after treatment with lethal doses of LPS with L-MyrARF6 2-13 or the ARF6 inhibitory activity negative D-MyrARF6 peptides. Interestingly, treatment with the D-enantiomer, while slightly slowing the rate of death of septic mice, had no effect on overall survival or serum TNF-α levels, suggesting that the antimicrobial peptide effect is limited to *in vitro* settings such as tissue culture and severely reduced or absent in our model of endotoxemia.

Discussion

We have provided evidence to suggest that a peptide composed of the amino terminus of ARF6, MyrARF6 2-13, interacts with LPS, and prevents LPS-induced signal transduction in a manner similar to antimicrobial peptides. The amino termini of ARF proteins are responsible for membrane association, so the observation that a peptide construct of this domain has bacterial membrane binding properties is somewhat unsurprising. We have also provided evidence to suggest that the antimicrobial activity is limited to *in vitro* assays because there is no evidence of inhibition of LPS-induced serum TNF-α levels or death in our *in vivo* endotoxemia model. Our observations suggest that researchers need to take great care in utilizing amino terminal ARF peptides as tools to probe ARF function in biological systems.

Importantly, we believe that the data presented in this appendix could be used to explain two key observations about LPS in TLR4 signaling throughout the literature. An ARF6 amino-terminal peptide has been used to suggest that ARF6 activation is necessary for MYD88-Adapter-Like protein (MAL) to bridge MYD88 to TLR4 and facilitate LPS-induced cytokine production [5]. However, in these experiments, LPS was co-incubated with the peptide in tissue culture and the data are likely a consequence of a direct interaction that sequesters LPS rather than the TLR4 signaling cascade. Similar experimental methods were also utilized to suggest that ARF6 is necessary for TLR4-Adapter-Protein (TRAM)-mediated TLR4 signaling [6]. Supporting the conclusion that ARF6 is not involved in LPS-induced cytokine production is our observation that siRNAs directed again ARF6 fail to inhibit LPS-induced cytokine production in endothelial cells but are able to inhibit LPS-induced permeability.

Although we observed no antimicrobial affect of either the L- or the D-MyrARF6 2-13 peptides in our endotoxemia assay, the treatments were administered in separate tissue compartments: LPS into the peritoneum, and the peptide intravenously. It is possible that if both were injected into the same tissue compartment then an antimicrobial affect may be observed. Collectively, the data presented in this appendix and throughout this dissertation suggests that two potential interactions between ARF6 and LPS exist: one of which is observed *in vitro* through a direct association with the N-terminus and LPS that prevents LPS-mediated signal transduction and another through MYD88 that facilitates LPS-induced VE-Cadherin internalization.

Materials and methods

Many of the experiments presented in this appendix were done concurrently or in a manner exactly the same as described in the methods as the manuscript printed earlier in this chapter. For siRNA, peptide synthesis, transwell permeability assay, ARF6 activation, cytokine analysis, and endotoxemia survival assay methods, please refer to the Materials and Methods section on p43-45.

Cadaverine displacement assay. This assay was adapted from previously published protocols [4]. Briefly, serial dilutions of denoted treatments were incubated in 10 μg/mL LPS and 1 μM bodipy cadaverine in 50 mM tris pH 7.4. Fluorescence was measured using a BioTek microplate fluorometer.

Minimal inhibitory concentration (MIC) determination. Serial dilutions in Luria broth of denoted peptides were incubated over night at 37°C with a 1:10,000 dilution of a stationary phase clinical isolate of *E. coli*. The absorbance of the cultures

was assessed with a BioTek microplate spectrophotometer and the MIC was defined as the lowest concentration by which 100% inhibition of bacterial growth was observed.

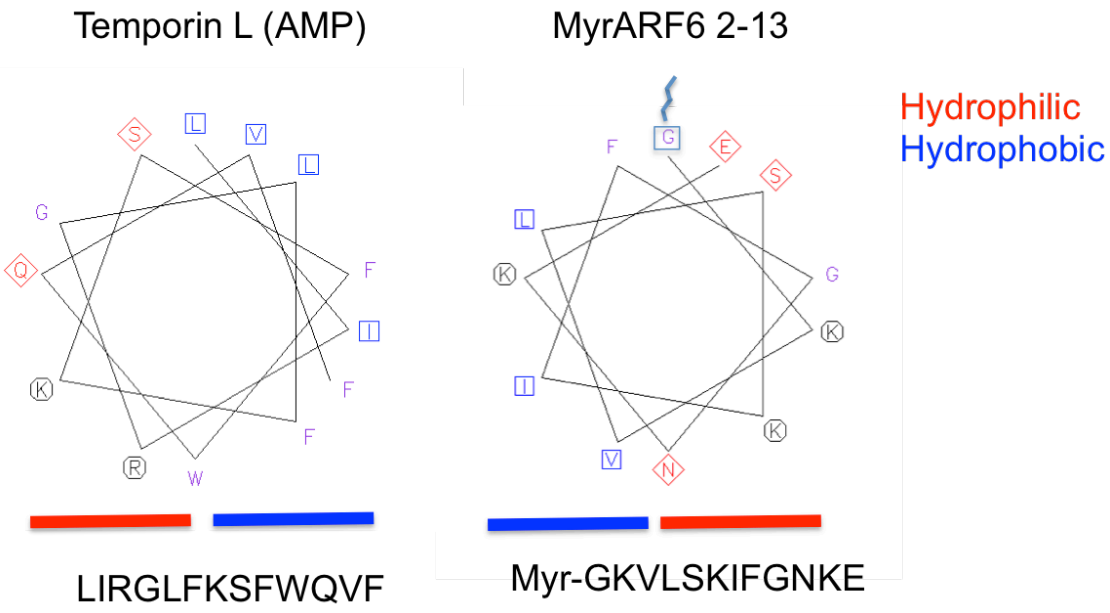

Figure 3.1 **MyrARF6 2-13 is an amphipathic helix that resembles the structure of an antimicrobial peptide.**

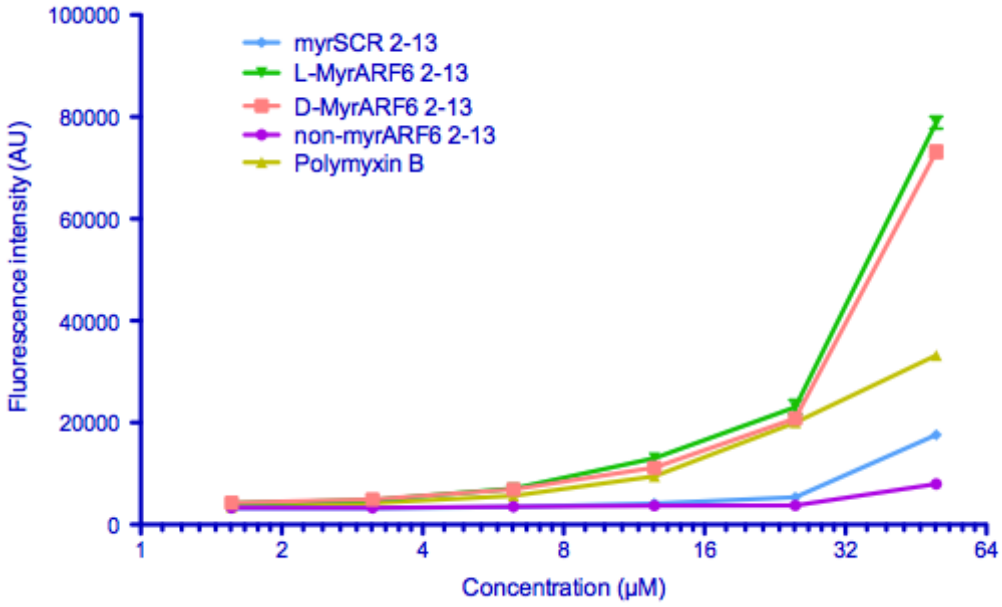

Figure 3.2 **MyrARF6 interacts with LPS.** LPS and BODIPY cadaverine were incubated with increasing concentrations of denoted treatments and fluorescence was measured using a microplate fluorometer.

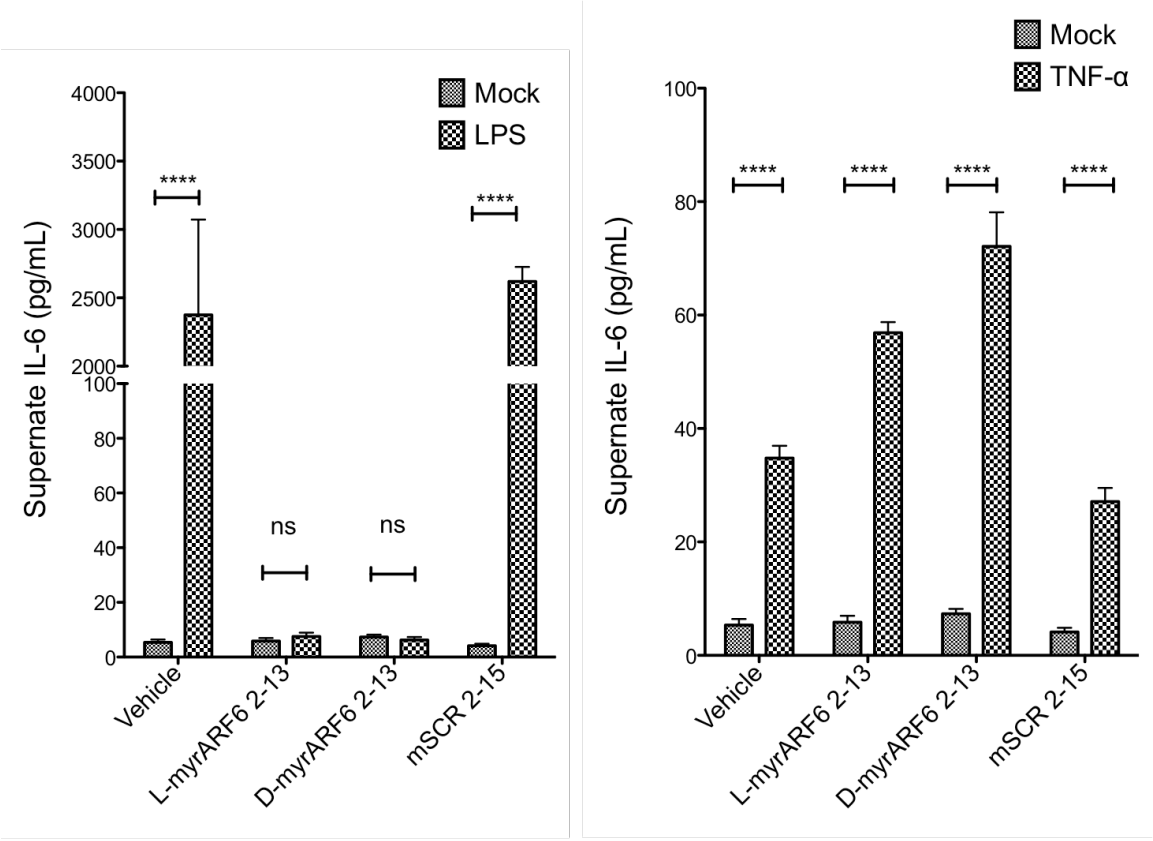

Figure 3.3 **MyrARF6 2-13 prevents LPS-induced, but not TNF-α-induced cytokine expression.** Endothelial cells were treated with (a) LPS or (b) TNF-α and denoted peptides. Supernatants were collected 5 hr post treatment and assessed for IL-6 expression via Millipore Milliplex analysis.

Table 3.1 **MIC Table of MyrARF6 2-13.** Denoted treatments were serially two-fold diluted in Luria broth and inoculated with 1:10,000 dilution of a clinical isolate of stationary phase *E. coli.* Bacteria were allowed to grow for 24 hr and the absorbance at OD 660 was assessed with a microplate reader. The lowest concentration of treatment that observed no difference in absorbance from media alone is reported in the table. NA = not applicable, used when bacteria grew at all tested concentrations.

	Vehicle	MyrSCR 2-13	L-MyrARF6 2-13	D-MyrARF6 2-13	Temporin L	Polymyxin B	Ciprofloxacin
E. coli	NA	NA	100uM	100uM	6.25uM	1.6uM	<0.1uM

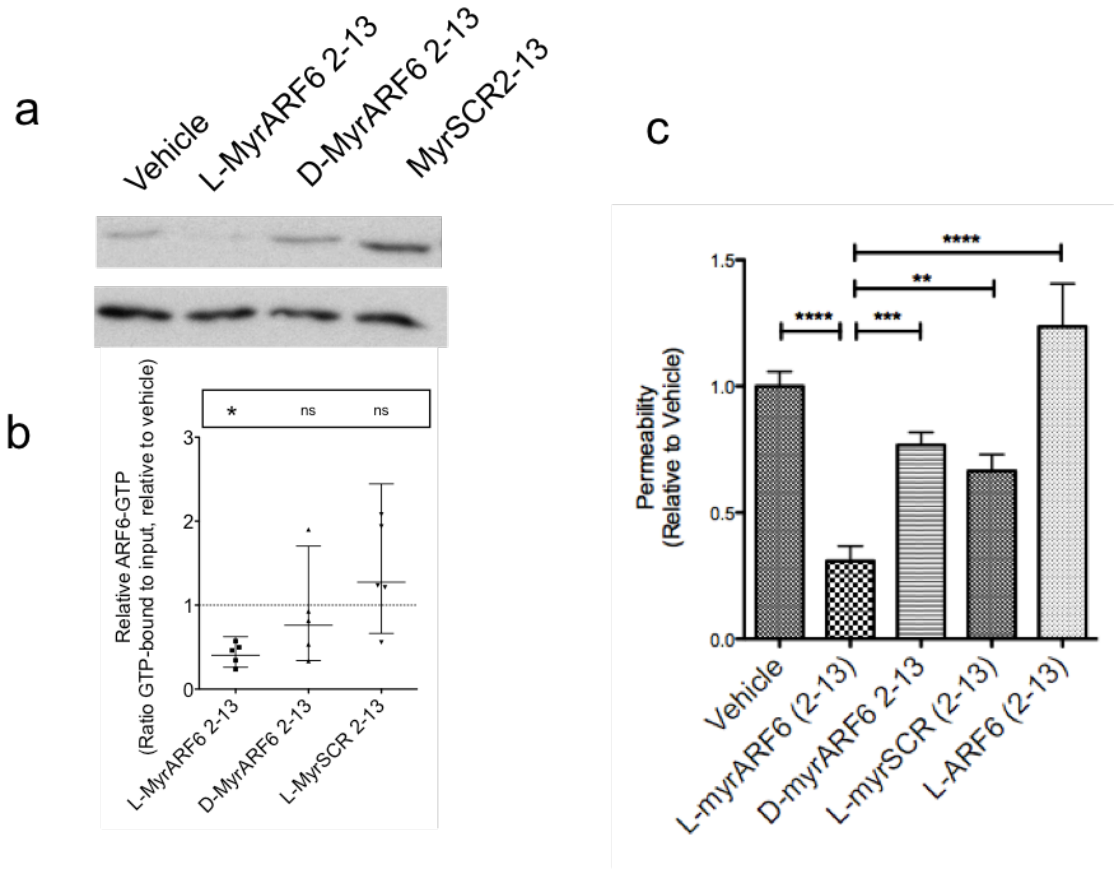

Figure 3.4 **The L-, but not D- enantiomer MyrARF6 peptide blocks ARF6 activity and reduces endothelial permeability. (a-b)** HMVEC-D were exposed to 25 μM treatments of the denoted peptides, or vehicle and lysates were assessed for the ratio of ARF6-GTP to total ARF6 in the cell lysate. Data are presented as the geometric mean and 95% confidence interval; asterisk denotes a statistically significant result in which the upper bound of the 95% confidence interval for the normalized ratio does not cross 1 (the null value). **(c)** HMVEC-D were exposed to the denoted treatments and assessed for their ability to inhibit leak of 40 kD FITC dextran.

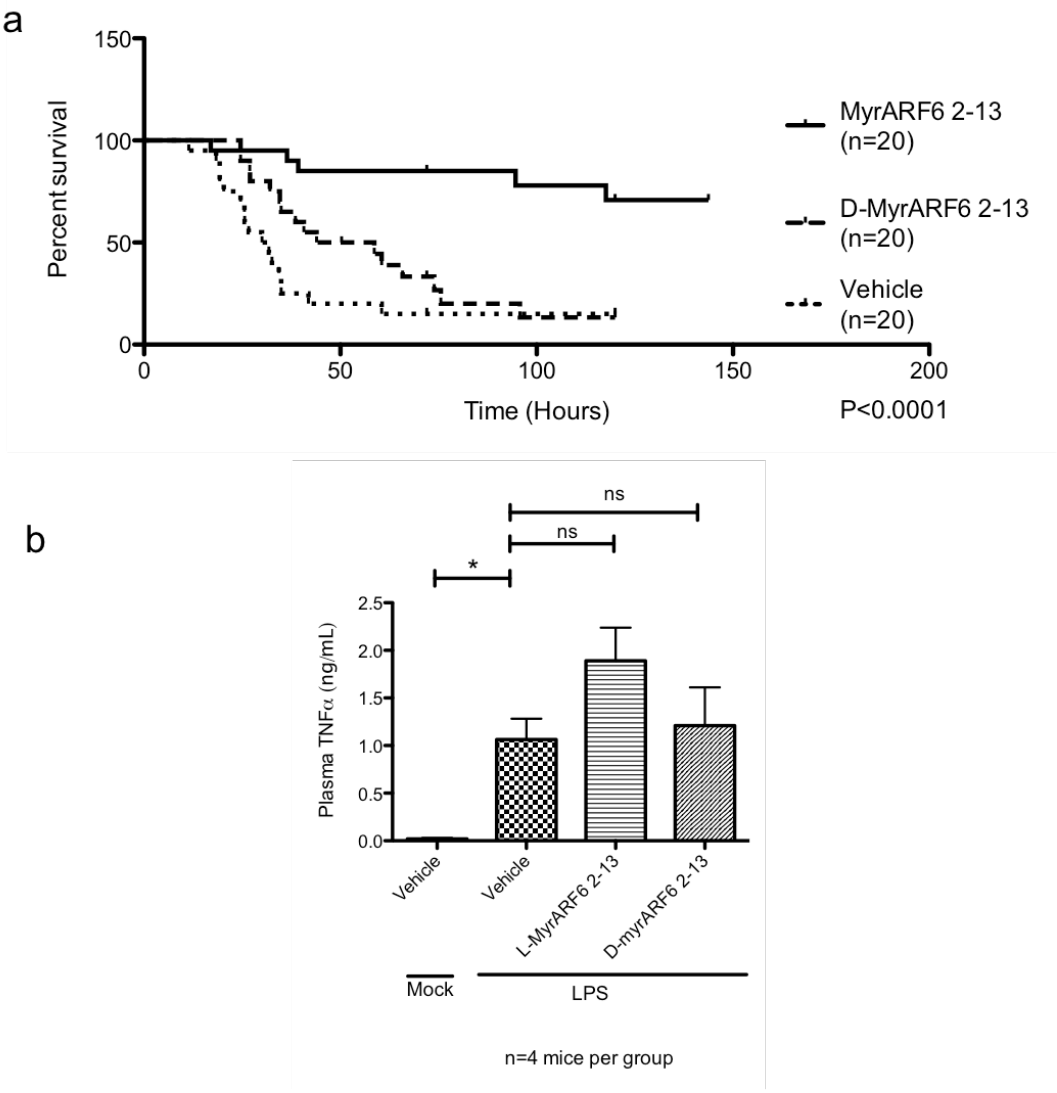

Figure 3.5 **Antimicrobial peptide activity, but not ARF6-inhibiory activity is dispensable for MyrARF6 2-13 mediated survival during endotoxemia.** Mice were anesthetized with ketamine and IP administered a lethal dose (25 mg/kg) of LPS concurrently with 40 mmol/kg-denoted peptide I.V. and monitored for survival **(a)** and plasma TNF-α concentration after 5 hr, n=4 mice per group **(b)**. The Mantel-Cox test **(a)** and one-way ANOVA with Dunnett's multiple comparisons tests **(b)** were used to assess statistical significance.

References

1. Gizachew, D.; Oswald, R., NMR structural studies of the myristoylated N-terminus of ADP ribosylation factor 6 (Arf6). *FEBS Letters* **2006,** *580* (17), 4296-301.

2. (a) Giuliani, A.; Pirri, G.; Rinaldi, A. C., Antimicrobial peptides: the LPS connection. *Methods in molecular biology (Clifton, NJ)* **2010,** *618*, 137-54; (b) Henriques, S. T.; Melo, M. N.; Castanho, M. A., Cell-penetrating peptides and antimicrobial peptides: how different are they? *The Biochemical journal* **2006,** *399* (1), 1-7.

3. Randazzo, P. A.; Terui, T.; Sturch, S.; Fales, H. M.; Ferrige, A. G.; Kahn, R. A., The myristoylated amino terminus of ADP-ribosylation factor 1 is a phospholipid- and GTP-sensitive switch. *The Journal of biological chemistry* **1995,** *270* (24), 14809-15.

4. Wood, S. J.; Miller, K. A.; David, S. A., Anti-endotoxin agents. 1. Development of a fluorescent probe displacement method optimized for the rapid identification of lipopolysaccharide-binding agents. *Combinatorial chemistry & high throughput screening* **2004,** *7* (3), 239-49.

5. Kagan, J. C.; Medzhitov, R., Phosphoinositide-mediated adaptor recruitment controls Toll-like receptor signaling. *Cell* **2006,** *125* (5), 943-955.

6. Van Acker, T.; Eyckerman, S.; Vande Walle, L.; Gerlo, S.; Goethals, M.; Lamkanfi, M.; Bovijn, C.; Tavernier, J.; Peelman, F., The small GTPase Arf6 is essential for the Tram/Trif pathway in TLR4 signaling. *The Journal of biological chemistry* **2013**.

CHAPTER 4

SUMMARY AND CONCLUSIONS

Vascular leak is a phenomenon observed in nearly all inflammatory pathologies. The resulting improper fluid balance between the vessels and the peripheral tissues is associated with diminished tissue and organ function, damage, and in some cases, death. There are many pro-inflammatory cues and they vary widely in structure and source. Examples include small, host-produced, bio-active molecules such as histamine and bradykinins [1], inflammatory cytokines such as IL-1β and TNF-α [2], and danger-associated molecular patterns (DAMPs) such as bacterial lipopolysaccharides and chromosomal HMGB1 [3], and others [4]. These pro-inflammatory cues all have specific receptors present in endothelial cells: GPCRs for histamine and bradykinins and single pass-enzyme linked receptors such as interleukin-1 receptor for IL-1β and the TLRs for most DAMPs. This thesis described the identification of a pathway in host endothelial cells by which MYD88 recruits ARNO and ARF6 to induce permeability by destabilizing VE-cadherin at the cell junction.

The characterization of ARF6 as a central mediator of vascular permeability in this dissertation was precipitated by the identification of ROBO4, a family member of the traditionally inhibitory axonal guidance receptors. Path-finding neurons structurally and behaviorally resemble angiogenic blood vessels and it was hypothesized that the stabilizing and inhibitory machinery described for neurons may be recycled for use in blood vessels. A screen was performed on mice that displayed enhanced endothelial instability and sprouting

defects to identify genes that resembled inhibitory receptors of neurons that were upregulated as a compensatory stabilizing mechanism [5]. One such molecule is a member of the inhibitory neural guidance receptor family, the roundabouts, and was subsequently named Robo4. The roundabout family of proteins is canonically stimulated by their ligands, Slits. Stimulation of the Robo4 receptor on endothelial cells by the Slit2 protein prevented endothelial migration in a manner similar to Slit2's effect on neurons. Slit2 also demonstrated Robo4-dependent inhibition of endothelial permeability [6]. Further characterization of the downstream Robo4 signaling pathway revealed that the cytoplasmic tail of Robo4 could interact with paxillin [7], a binding partner of the ARF6 GAP, GIT1[8]. The ability of GIT1 to deactivate ARF6 upon Slit2 stimulation was demonstrated to be necessary for Robo4's stabilizing effects of the endothelium [7]. We then asked if the converse was true, if Robo4 stabilizes the endothelium by deactivating ARF6, could it be possible that pro-inflammatory cues destabilize the endothelium by activating ARF6? Indeed, in Chapters 2 and 3, we showed that the destabilizing cues IL-1β and LPS activate ARF6 and that ARF6 activation is both necessary and sufficient to induce endothelial permeability.

To determine how IL-1β and LPS activate ARF6, we interrogated their highly similar and well-characterized signaling pathways. Both of their receptors recruit MYD88 to facilitate an IL-1R-associated kinase (IRAK)-initiated signaling cascade culminating in the activation of Iκ B kinase complex (IKK) to phosphorylate Iκ B-α. This allows NF-κB and other transcription factors to transport into the nucleus and facilitate the expression of inflammatory genes such as cytokines and cell adhesion molecules. However, inhibition of new transcription and translation did not block IL-1β-induced permeability, suggesting permeability and ARF6 activation occurred upstream of changes in gene expression. siRNAs directed against MYD88 but not IRAK blocked IL-1β-induced ARF6 activation, suggesting

that MYD88 may be acting as a scaffold for an ARF6 GEF. Immunoprecipitation revealed that MYD88 associated with ARNO, and that this MYD88-ARNO interaction facilitated ARF6 activation.

We showed that a MYD88-ARNO-ARF6-cadherin signaling axis was responsible for enhancing endothelial permeability, but importantly, we also observed that this enhancement was independent of the other components of the inflammatory response such as expression of cytokines and cell adhesion molecules. The separation of pathology from the cytokine response is a unique observation because most of the proposed treatments for inflammatory diseases such as arthritis and sepsis include broad-spectrum anti-inflammatories that directly target cytokines or block their expression. Indeed, the presence of inflammatory cytokines correlates well with pathology and is often sufficient to induce vascular leak and pathology. However, what we have described is a novel mechanism by which presence of inflammatory cues can be separated from the pathogenesis. This allows for the development of treatments to focus on the branch of the immune signaling pathways responsible for vascular leak to avoid side effects associated with broad-spectrum anti-inflammatories. Our data also suggest that vascular leak itself, and not other ancillary components of the inflammatory response such as the presence of cytokines and inflammatory cells, is a driver of the pathogenesis in inflammatory diseases such as arthritis and endotoxemia. It is possible that the inhibition of this axis may also prevent pathology in other inflammatory diseases where substantial vascular leak has been observed such as trauma, epilepsy, and multiple sclerosis [9]. Future experiments should be directed toward elucidating the role of the ARF6 pathway in these diseases where vascular leak is an integral part of the pathogenesis.

While we have identified ARF6 as a key regulator of VE-cadherin deposition and vascular permeability, the components downstream of ARF6 that facilitate this response

remain unidentified and are an important area of study. There are a number of potential models for ARF6-mediated VE-Cadherin destabilization. ARF6 is reported to be a key driver of PIP_2 synthesis through its activation of PIP5K [10]. PIP_2 is a commonly used second messenger and PIP_2 synthesized by PIP5K has been shown to enhance adhesion strength of N-Cadherin in fibroblasts [11]. It is possible a similar mechanism may occur between in endothelial cells. Another possibility is that ARF6 might modulate reactive oxygen species (ROS)-sensitive phosphatases. ARF6 is a key regulator of ROS in neutrophils and endothelial cells [12]. ARF6-mediated ROS activity may target the catalytic cysteine residue on VE-PTP or other endothelial PTPs and prevent phosphatase activity, thereby disrupting the phosphorylation status and stability of VE-Cadherin [13]. Finally, it has also been demonstrated that ARF6 GTP status is sufficient to induce positive membrane curvature [14]. Therefore, ARF6 may be the component of the VE-cadherin endocytic machinery responsible for generation of the positive membrane curvature necessary to form the endocytic vesicle.

One active area of study in our group is determining the extent to which the MYD88-ARNO-ARF6-cadherin cascade is conserved among cell types. MYD88 is a widely expressed scaffolding protein present in epithelial cells, leukocytes, and many others [15]. ARF6 is also expressed in many cell types [16]. It is possible that such a cascade may have similar functions in other MYD88 expressing cells and preliminary data suggest ARF6 may regulate barrier function in epithelial cells. In a model of LPS-induced acute lung injury, administration of a small molecule inhibitor of ARNO/ARF6 signaling directly to the lung epithelium of mice blocked cellular infiltration and albumin flux into bronchial-alveolar lavage fluid (data not shown). However, it is not clear if this response is due to an effect of the small molecule interacting with the endothelium. Further experiments with lung alveolar epithelial cell-specific genetic knockouts of ARF6 are in progress to determine cell-

specificity of this phenotype. Additionally, N-cadherin in leukocytes is important for attachment to endothelial cells, and blockade of this cascade may facilitate the enhancement of N-cadherin surface localization on leukocytes and increase attachment to endothelial cells. However, we detected no statistically significant changes in IL-1β-induced leukocyte attachment to endothelial cells [17] nor enhanced extravasation of leukocytes during endotoxemia (data not shown) upon ARF6 inhibition, suggesting that ARF6 may not be an important regulator of leukocyte adhesion.

Collectively, the observations contained within this dissertation have identified ARF6 as a key regulator of vascular permeability that is independent of canonical inflammatory signaling leading to cytokine expression. They have also demonstrated a novel way to prevent inflammatory pathology: by reducing vascular leak. However, our observations have also raised many questions. What other cell types use this axis and for what purposes? What are the downstream effectors of ARF6? What other diseases can be ameliorated by enhancing vascular stability? These questions are currently being investigated in our laboratory. Their answers will lead to novel insights into the mechanisms by which inflammation induces pathology, the biology of inflammatory cytokines, ARF6, cadherins, and vesicular trafficking, and possible new treatment opportunities for inflammatory diseases.

References

1. Ehringer, W. D.; Edwards, M. J.; Miller, F. N., Mechanisms of alpha-thrombin, histamine, and bradykinin induced endothelial permeability. *Journal of cellular physiology* **1996,** *167* (3), 562-9.

2. Stolpen, A. H.; Guinan, E. C.; Fiers, W.; Pober, J. S., Recombinant tumor necrosis factor and immune interferon act singly and in combination to reorganize human vascular endothelial cell monolayers. *The American Journal of Pathology* **1986,** *123* (1), 16-24.

3. Fitzner, N.; Clauberg, S.; Essmann, F.; Liebmann, J.; Kolb-Bachofen, V., Human skin endothelial cells can express all 10 TLR genes and respond to respective ligands. *Clinical and vaccine immunology : CVI* **2008,** *15* (1), 138-46.

4. Mehta, D.; Malik, A. B., Signaling mechanisms regulating endothelial permeability. *Physiological reviews* **2006,** *86* (1), 279.

5. Park, K. W.; Morrison, C. M.; Sorensen, L. K.; Jones, C. A.; Rao, Y.; Chien, C. B.; Wu, J. Y.; Urness, L. D.; Li, D. Y., Robo4 is a vascular-specific receptor that inhibits endothelial migration. *Developmental biology* **2003,** *261* (1), 251-267.

6. (a) Jones, C.; London, N.; Chen, H.; Park, K.; Sauvaget, D.; Stockton, R.; Wythe, J.; Suh, W.; Larrieu-Lahargue, F.; Mukouyama, Y., Robo4 stabilizes the vascular network by inhibiting pathologic angiogenesis and endothelial hyperpermeability. *Nature Medicine* **2008,** *14* (4), 448-453; (b) London, N. R.; Zhu, W.; Bozza, F. A.; Smith, M. C. P.; Greif, D. M.; Sorensen, L. K.; Chen, L.; Kaminoh, Y.; Chan, A. C.; Passi, S. F.; Day, C. W.; Barnard, D. L.; Zimmerman, G. A.; Krasnow, M. A.; Li, D. Y., Targeting Robo4-Dependent Slit Signaling to Survive the Cytokine Storm in Sepsis and Influenza. *Science Translational Medicine* **2010,** *2* (23), 23ra19-23ra19.

7. Jones, C.; Nishiya, N.; London, N.; Zhu, W.; Sorensen, L.; Chan, A.; Lim, C.; Chen, H.; Zhang, Q.; Schultz, P.; Hayallah, I.; Thomas, K.; Famulok, M.; Zhang, K.; Ginsberg, M.; Li, D., Slit2–Robo4 signalling promotes vascular stability by blocking Arf6 activity. *Nature cell biology* **2009**.

8. Nishiya, N.; Kiosses, W.; Han, J.; Ginsberg, M., An α4 integrin–paxillin–Arf-GAP complex restricts Rac activation to the leading edge of migrating cells. *Nature cell biology* **2005,** *7* (4), 343-352.

9. (a) Chodobski, A.; Zink, B. J.; Szmydynger-Chodobska, J., Blood-brain barrier pathophysiology in traumatic brain injury. *Translational stroke research 2* (4), 492; (b) van Vliet, E. A.; da Costa Araújo, S.; Redeker, S.; van Schaik, R.; Aronica, E.; Gorter, J. A., Blood-brain barrier leakage may lead to progression of temporal lobe epilepsy. *Brain : a journal of neurology* **2007,** *130* (Pt 2), 521-34; (c) Minagar, A.; Alexander, J. S., Blood-brain barrier disruption in multiple sclerosis. *Multiple sclerosis (Houndmills, Basingstoke, England)* **2003,** *9* (6), 540-9.

10. Honda, A.; Nogami, M.; Yokozeki, T.; Yamazaki, M.; Nakamura, H.; Watanabe, H.; Kawamoto, K.; Nakayama, K.; Morris, A. J.; Frohman, M. A.; Kanaho, Y., Phosphatidylinositol 4-phosphate 5-kinase alpha is a downstream effector of the small G protein ARF6 in membrane ruffle formation. *Cell* **1999,** *99* (5), 521-32.

11. El Sayegh, T. Y.; Arora, P. D.; Ling, K.; Laschinger, C.; Janmey, P. A.; Anderson, R. A.; McCulloch, C. A., Phosphatidylinositol-4,5 bisphosphate produced by PIP5KIgamma regulates gelsolin, actin assembly, and adhesion strength of N-cadherin junctions. *Molecular biology of the cell* **2007,** *18* (8), 3026-38.

12. (a) Ikeda, S.; Ushio-Fukai, M.; Zuo, L.; Tojo, T.; Dikalov, S.; Patrushev, N. A.; Alexander, R. W., Novel role of ARF6 in vascular endothelial growth factor-induced signaling and angiogenesis. *Circulation Research* **2005,** *96* (4), 467; (b) Ushio-Fukai, M., VEGF signaling through NADPH oxidase-derived ROS. *Antioxidants & Redox Signaling* **2007,** *9* (6), 731-739; (c) Dana, R. R.; Eigsti, C.; Holmes, K. L.; Leto, T. L., A regulatory role for ADP-ribosylation factor 6 (ARF6) in activation of the phagocyte NADPH oxidase. *Journal of Biological Chemistry* **2000,** *275* (42), 32566.

13. (a) Ushio-Fukai, M., Compartmentalization of redox signaling through NADPH oxidase-derived ROS. *Antioxidants & Redox Signaling* **2009,** *11* (6), 1289-99; (b) Monaghan-Benson, E.; Burridge, K., The regulation of vascular endothelial growth factor-induced microvascular permeability requires Rac and reactive oxygen species. *J Biol Chem* **2009,** *284* (38), 25602-11; (c) Vestweber, D.; Winderlich, M.; Cagna, G.; Nottebaum, A., Cell adhesion dynamics at endothelial junctions: VE-cadherin as a major player. *Trends in cell biology* **2009,** *19* (1), 8-15.

14. Lundmark, R.; Doherty, G. J.; Vallis, Y.; Peter, B. J.; McMahon, H. T., Arf family GTP loading is activated by, and generates, positive membrane curvature. *The Biochemical journal* **2008,** *414* (2), 189-94.

15. Janssens, S.; Beyaert, R., A universal role for MyD88 in TLR/IL-1R-mediated signaling. *Trends in biochemical sciences* **2002,** *27* (9), 474-482.

16. Donaldson, J. G.; Jackson, C. L., ARF family G proteins and their regulators: roles in membrane transport, development and disease. *Nature Reviews Molecular Cell Biology* **2011,** *12* (6), 362-375.

17. Zhu, W.; London, N. R.; Gibson, C. C.; Davis, C. T.; Tong, Z.; Sorensen, L. K.; Shi, D. S.; Guo, J.; Smith, M. C.; Grossmann, A. H.; Thomas, K. R.; Li, D. Y., Interleukin receptor activates a MYD88-ARNO-ARF6 cascade to disrupt vascular stability. *Nature* **2012,** *492* (7428), 252-5.